THE JOURNAL OF PHYSICAL CHEMISTRY B

ARTICLE

pubs.acs.org/JPCB

Radiation Induced Redox Reactions and Fragmentation of Constituent Ions in Ionic Liquids. 1. Anions

Ilya A. Shkrob,*[,†] Timothy W. Marin,[†,‡] Sergey D. Chemerisov,[†] and James F. Wishart[§]

[†]Chemical Sciences and Engineering Division, Argonne National Laboratory, 9700 S. Cass Ave, Argonne, Illinois 60439, United States

[‡]Chemistry Department, Benedictine University, 5700 College Road, Lisle, Illinois 60532, United States

[§]Chemistry Department, Brookhaven National Laboratory, Upton, New York 11973-5000, United States

Supporting Information

ABSTRACT: Room temperature ionic liquids (IL) find increasing use for the replacement of organic solvents in practical applications, including their use in solar cells and electrolytes for metal deposition, and as extraction solvents for the reprocessing of spent nuclear fuel. The radiation stability of ILs is an important concern for some of these applications, as previous studies suggested extensive fragmentation of the constituent ions upon irradiation. In the present study, electron paramagnetic resonance (EPR) spectroscopy has been used to identify fragmentation pathways for constituent anions in ammonium, phosphonium, and imidazolium ILs. Many of these detrimental reactions are initiated by radiation-induced redox processes involving these anions. Scission of the oxidized anions is the main fragmentation pathway for the majority of the practically important anions; (internal) proton transfer involving the aliphatic arms of these anions is a competing reaction. For perfluorinated anions, fluoride loss following dissociative electron attachment to the anion can be even more prominent than this oxidative fragmentation. Bond scission in the anion was also observed for NO_3^- and $B(CN)_4^-$ anions and indirectly implicated for BF_4^- and PF_6^- anions. Among small anions, $CF_3SO_3^-$ and $N(CN)_2^-$ are the most stable. Among larger anions, the derivatives of benzoate and imide anions were found to be relatively stable. This stability is due to suppression of the oxidative fragmentation. For benzoates, this is a consequence of the extensive sharing of unpaired electron density by the π-system in the corresponding neutral radical; for the imides, this stability could be the consequence of N−N $\sigma^2\sigma^{*1}$ bond formation involving the parent anion. While fragmentation does not occur for these "exceptional" anions, H atom addition and electron attachment are prominent. Among the typically used constituent anions, aliphatic carboxylates were found to be the least resistant to oxidative fragmentation, followed by (di)alkyl phosphates and alkanesulfonates. The discussion of the radiation stability of ILs is continued in the second part of this study, which examines the fate of organic cations in such liquids.

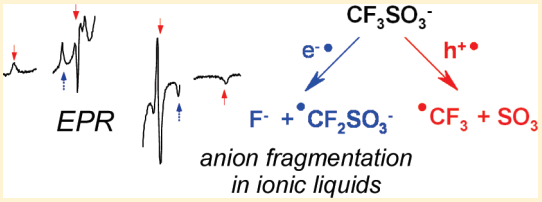

1. INTRODUCTION

Room temperature ionic liquids (ILs) are fascinating new solvents. Compositionally, these are salts of irregularly shaped (organic) ions that have low melting points.[1−4] Such liquids combine tunable physicochemical properties, low volatility, and good electric conductivity, which makes these solvents attractive choices for many applications. They find utility in chemical synthesis,[5] photovoltaic devices,[6] and electrolytic cells,[7] lubrication and protection of surfaces,[8] cellulose processing,[9] and metal ion extractions.[10−13] Redox reactions involving the constituent ions interfere with some of these applications and, as such, are of considerable interest. These reactions are particularly important in electrolytic, photolytic, and radiation-induced degradation of the ILs.

This article continues a series of mechanistic studies of IL radiolytic damage from our two laboratories.[14−16] A prime motivation for studying IL radiolysis is the growing use of ILs for radionuclide extractions, which involves d- and f- metal ions and certain oxoanions (such as pertechnetate) involved in the "wet" processing of spent nuclear fuel.[17] Hydrophobic ILs can substitute for organic solvents in these practically important liquid−liquid extractions.[10,18−22] The main advantage of ILs over traditional molecular organic solvents is the ease of ion solvation in such liquids, which frequently results in superior separations efficacy and obviates the need for solvent modifiers and phase transporters.[11] The main disadvantage of ILs is the frequent occurrence of interphase ion exchange, leading to the loss of the constituent ions to the aqueous phase, third phase formation, and gradual deterioration of the IL solvent.[10,18,19] Recent studies suggest that this disadvantage can be surmounted by the judicious choice of the constituent ions;[19,23,24] however, there is another challenge that appears to be even more formidable. The strong ion solvation that drives the ion extraction equilibria toward the IL phase greatly complicates stripping of metal ions from the ILs following their forward extraction.[24] For many systems, electrolytic stripping could be a better option.[22,25]

Received: January 11, 2011
Revised: February 8, 2011
Published: March 21, 2011

This puts additional requirements on the IL solvent, as it needs to double as the extraction solvent and the electrolyte. The latter role brings to the fore the redox stability of the solvent, in addition to its chemical and radiolytic durability.[16] Thus, to serve as possible replacements for traditional extraction systems, hydrophobic IL solvents may need to address conflicting requirements, and the separation schemes based on ILs could differ substantially from those used today. During nuclear separations, ILs could encounter high radiation fields generated by decaying radionuclides, so their reusability and robustness under such conditions are of concern, as they are for present extraction systems based on conventional solvents. Radiation damage to the solvent accumulated throughout its continuous use may compromise the performance of an extraction system, e.g., by generation of products interfering with extraction specificity or efficiency. Examples of such detrimental radiation-induced changes have recently been reported. For example, irradiation of 1-butyl-3-methylimidazolium (C_4mim)PF_6 or C_4mim bistriflimide (NTf_2^-; hereafter, Tf designates the triflyl, CF_3SO_2, group) containing an ionophore for Sr^{2+} extractions was shown to produce acids that interfere with Sr^{2+} ion binding to this ionophore in the IL (as the hydronium competes with the Sr^{2+} ion), although the effectiveness of the extraction could be restored by washing the IL with water.[26,27] Furthermore, radiolytic fragmentation of the bistriflimide anion yields SO_x species that precipitate strontium sulfate or sulfite at the water−IL interface.[28] These results underscore the importance of correctly selecting specific ionic liquids for nuclear separation tasks.

Chromatography, NMR, and mass spectrometry studies[29−31] on two major classes of hydrophobic ionic liquids (based on alkylated ammonium and imidazolium cations) reveal appreciable fragmentation in the constituent cations (C^+) and anions (A^-), such as BF_4^-, PF_6^-, TfO^-, and NTf_2^- at doses of 1.2−2 MGy, approximately the upper limit for anticipated radiation exposures for processing systems. The fractional degradation of the anions in C_4mim A^- liquids ranged from 0.24 for BF_4^- to 0.47 in NTf_2^- (see Table 6 in ref 31), and the overall degradation of the bistriflimide anion in C_4mim NTf_2 was estimated as 2.2 species per 100 eV absorbed energy.[31] Given that the typical ionization yield in an organic liquid is 3−5 ion pairs per 100 eV, this means that a significant fraction of such ionization/excitation events may result in the fragmentation of the anions. Product analyses also show the loss of hydrogen in both the imidazolium ring and in the long arms, the loss of the entire aliphatic arm, the dissociation of N−S bonds in the NTf_2 radical, dissociation C−S bonds in NTf_2^- and TfO^- anions, and dissociation of P−F and B−F bonds in PF_6^- and BF_4^- anions, respectively.[31] The released fragment radicals can recombine and disproportionate, yielding volatile, acidic, or metal-binding products, causing deteriorated solvent performance. In common organic solvents that are used for nuclear separations (such as *n*-dodecane), this *solvent* degradation is seldom a concern; a far greater concern is the deterioration of the *extracting agent* that has lower ionization potential (IP) than the bulk solvent, resulting in channeling of the excess charges and excitation to the extracting agent, thereby causing its fragmentation.[14,32] Due to the much lower IPs of the constituent anions in ILs as compared to those for alkanes, this situation is reversed:[14,32,33] the damage to the extracting agent is minimal, whereas the solvent takes the brunt of the damage. These properties make the radiation stability of the *solvent* a prime objective. Ideally, the fragmentation of the constituent ions should be minimal. Is such a goal obtainable? Can a radiation-resistant IL be rationally designed? Both of these questions are addressed in this study.

The first step toward the realization of the latter goal is finding how the ions fragment upon radiolysis and what controls their stability. To this end, electron paramagnetic resonance (EPR) spectroscopy was used to detect radicals and radical ions following their radiolytic generation in frozen ILs and their crystalline analogs. As the ILs consist of cations and anions that have quite different properties with regard to their radiation chemistry, we have organized our report accordingly: the present study deals almost exclusively with the fate of the anions, whereas part 2[33] addresses the reactions of derivatized imidazolium cations (as currently such imidazolium ILs are the most extensively studied class of ILs). While such organization of the narrative is logical, it presents difficulty to presenting results, because it presumes that the anion fragmentation pathways are similar in all ILs and ignores the fact that secondary radical reactions differ in different classes of ILs, which, in turn, affects their stability. Hence, a single-minded focus on anion chemistry would be misleading, and some cation chemistry needs be addressed along the way.

A closely related issue is the role of impurities in the ILs that, like all organic liquids, contain traces of other compounds. Due to common approaches used in the synthesis of various ILs, the contamination frequently involves halide anions, X^-, which have low IPs, and consequently serve as hole traps, even at the trace level. As shown elsewhere,[33] a protic impurity (involving free or clustered water molecules) also has a significant effect, as it serves as the lowest-energy electron trap. Even trace levels of such an impurity can significantly affect the IL radiation chemistry through generation of mobile, reactive $H^\bullet$ atoms that readily abstract hydrogen and add to π-rings of aromatic ions.

In aromatic ILs (such as those composed of imidazolium and pyridinium ions) the cations readily trap electrons, competing with the electron-accepting anions; this competition is lacking for aliphatic ILs.[14,32] Thus, the two major classes of ILs can exhibit rather different chemistries even when the constituent anion is the same. For all of the above reasons, providing an exhaustive catalog of radical reactions would be a daunting task. Instead, our approach is to survey a wide variety of IL classes to identify general trends that can be used in the rational design of ILs for durable separations systems, and by extension, for other applications involving extreme redox conditions.

2. GENERAL CONSIDERATIONS

Hereafter we adapt the nomenclature in which the residue of the 1-methyl-3-alkyl-imidazolium cation with respect to substitution in the *n*-th atom in the ring is designated as Q_n. In this nomenclature, the 2-imidazolyl radical is $Q_2H^\bullet$, the 2-ylidene carbene is $Q_2^{\bullet\bullet}$, etc. Before going into a more detailed description, it is useful to convey some general observations relating to all of the IL systems examined. Ionization of the ILs generates short-lived primary charges: excess electrons and "holes" (electron deficiencies consisting of monomer or multimer radical cations). In aliphatic ILs, trapped electrons (analogous to F-centers in ionic solids,[34] in which the interstitial electron is stabilized by electrostatic interactions with several cations) can be observed on time scales of up to a few microseconds.[35−38] In imidazolium ILs, these excess electrons are short-lived (fully decaying on a tens-of-picosecond time scale).[39] As shown in part 2 of this study,[33] in the majority of imidazolium ILs, the cation ($C^+ = Q_2H^+$) readily accepts the excess electron, forming the

dx.doi.org/10.1021/jp2003062 |J. Phys. Chem. B 2011, 115, 3872–3888

Scheme 1. Typical Cation-Derived Radicals Observed by EPR in Irradiated 1-Methyl-3-alkylimidazolium ILs (Section 2)

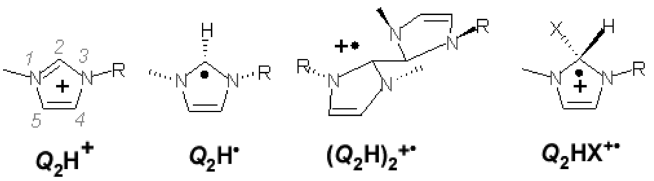

Table 1. DFT Estimates for Adiabatic Ionization Potentials, Bonding Energies for (Pseudo)Halide Anions, and Dissociation Energies (Reaction 1b) for Selected Anions

anion, A^-	$IP_{ad}(A^-)$, eV	$A^- + A^\bullet$, eV[a]	$D(R^\bullet+B)$, eV[c]
thiosalicylate	3.36		−0.026
benzoate	3.44		−0.006
picolinate	3.56		−0.34
bromide	3.60	1.44	
salicylate	3.64		−0.062
acetate	3.65		−0.63
chloride	3.70	1.50	
maleimide	3.90	0.86	
phthalimide	3.98	0.58	
dicyanamide	4.06	0.86	
succinimide	4.12	1.02	
methyl sulfate	4.26		1.04
tosylate	4.29		1.36
$(MeO)_2PO_2$	4.43		1.08
$MeOSO_3$	4.62		0.77
triflate	5.20		0.30
NTf_2[b]	5.50		
$B(ox)_2$[b]	6.30		−0.20
BF_4	7.31		
PF_6	8.02		

[a] For (pseudo)halides only. [b] ox = oxalate, Tf = CF_3SO_2. [c] Dissociation energy for reaction 1b; 3,5-dimethylbenzoate (−0.017), naphthalene-2,3-dicarboxylate (−0.30), 1,2,3-benzenetricarboxylate (−0.39), phthalate (−0.43), terephthalate (−0.91), 1,2,4,5-benzenetetracarboxylate (−1.67); α-alanine (−0.73), glycylglycine (−1.05), histidine (−0.95).

corresponding 2-imidazolyl σ−radical $Q_2H^\bullet$ with trigonal carbon-2 and nitrogen-1,3 atoms (Scheme 1).

However, in some imidazolium ILs (in particular, those that involve NTf_2^- and TfO^- anions), this neutral radical forms a C(2)−C(2) $\sigma^2\sigma^{*1}$ dimer radical cation $(Q_2H)_2^{+\bullet}$ (sketched in Scheme 1) with the parent imidazolium cation.[15,16,33] Due to the high electron affinity (EA) of the imidazolium cation and relatively low gas-phase IP of the anions (see Table 1 for the estimated adiabatic IPs), the "hole" can be expected to reside on these anions. "Ionization" of such ILs can be thought of as charge-transfer-to-solvent reaction:[15,39] electron detachment from the anion that is followed by the attachment of the released electron to the parent cation or (if the parent anion has a large EA) to another anion. Even if the parent cation is ionized (suffering direct radiolytic loss of an electron) to form the corresponding radical dication $(Q_2H)^{2+\bullet}$, the latter species, due to π-conjugation in the aromatic ring, could be sufficiently stable to transfer positive charge to a neighboring anion before undergoing deprotonation.[14] For aliphatic cations and imidazolium cations with long aliphatic arms, the charge-transfer mechanism stated above does not apply, and instead a hydrogen atom loss radical in the aliphatic arm (denoted $R^\bullet(C^+)$ in the following) is generated. Nevertheless, even in such systems, radiolytically induced electron detachment from the parent anion remains a major reaction channel.

Table 2. Radical Products Derived from the Constituent Anions and Identified in the Frozen ILs Using EPR Spectroscopy[a]

anion	radicals observed
X^-[b]	$X_2^{-\bullet}$
HSO_3^-	$H^\bullet$
NO_3^-	$NO_3^{2-\bullet}$, $NO_2^\bullet$, $NO_2^{2-\bullet}$
$CR_3CO_2^-$[c]	$^\bullet CR_3$, $^\bullet CR_2CO_2^-$
$CR_3SO_3^-$[c]	$^\bullet CR_3$, $^\bullet CR_2SO_3^-$, $CR_3SO_3^\bullet$
$CF_3CF_2CO_2^-$	$^\bullet CF_2CF_2CO_2^-$, $CF_3{}^\bullet CFCO_2^-$
$CH_3OSO_3^-$	$^\bullet CH_2OH$, $^\bullet CH_2OSO_3^-$, $CH_3OSO_3^\bullet$
$(CH_3O)_2PO_2^-$	$^\bullet CH_2OH$
$B(CN)_4^-$	$^\bullet B(CN)_2$, $B(CN)_3^{-\bullet}$
$B(ox)_2^-$[d]	$(ox)BO^\bullet C{=}O$
NTf_2^-	$^\bullet CF_3$, $^\bullet CF_2SO_2NTf^-$, $^\bullet NTf_2$

[a] The deprotonated forms of the radicals are given. [b] X = Br or $N(CN)_2$; [c] R = H or F. [d] ox = oxalato, from ref 15.

A large subset of the simple anions that are used in IL synthesis can be represented as RB^-, where R− is an alkyl or alkoxy group (or their perfluorinated analogs) and −B is an inorganic base (such as $-SO_3^-$, $-CO_2^-$, $-PO_2^{2-}$). One-electron oxidative decarboxylation and dephosphorylation involving alkyl and aryl carboxylates and phosphates, respectively, are well-known in organic chemistry, electrochemistry, and biochemistry (e.g., Kolbe reaction),[40] and these better-known reactions exemplify a more general pattern of the loss of base upon neutralization:

$$RB^- + h^{+\bullet} \rightarrow \{RB^\bullet\}^* \quad (1a)$$

$$\{RB^\bullet\}^* \rightarrow R^\bullet + B \quad (1b)$$

which yields the corresponding fragment radical $R^\bullet$ (Table 2). As demonstrated in section 4, reaction 1a occurs in most of the ILs composed of RB^- anions, even if the ground state of the intermediate radical $RB^\bullet$ is relatively stable. This is explained by the fact that reaction 1a is strongly exergonic and the neutral radical $RB^\bullet$ is generated in an electronically and/or vibrationally excited state. The potential presence of water increases the likelihood of reaction 1b involving the relaxed $RB^\bullet$ radical through the hydration of B with the formation of acids:

$$B + 2H_2O \rightarrow HOB^- + H_3O^+ \quad (1c)$$

It is precisely reaction 1c that causes a radiation-induced increase in proticity.[26,27,33] The fluorination of the RB^- anions (which is a popular approach to increasing hydrophobicity and chemical durability of ILs) has little effect on the facility of reaction 1a. For alkyl and alkoxy RB^- anions, we observed deprotonation from the aliphatic moiety as a reaction competing with reaction 1b. Table 2 summarizes the radicals observed for the different anions we examined.

The observations of Moisy and co-workers[30,31] are typical; in ILs most of the commonly used constituent anions do undergo appreciable fragmentation upon radiolysis. The stabilization of the anion could be achieved either via (i) preventing reaction 1a through increasing the IP of the constituent anions (Table 1) or (ii) stabilization of the intermediate radical. In the former case, the overall radiation stability of the IL is not necessarily increased, as the cations are ionized instead, resulting in their fragmentation.[14,33] Nonetheless, the formation of undesirable products (acids, nonspecific complexants, volatile molecules) can be prevented. However, our EPR studies suggest that increasing the IP of the anion has little effect on its radiation stability, as the ionization events in radiolysis are energetic (5−20 eV) and reaction 1a still occurs. A more successful approach was using large anions that have conjugated π-systems, as the corresponding radicals and their excited states are more stable (section 4.4).

This paper is organized as follows. In sections 4.1−4.3 we consider "simple" anions commonly used in ionic liquids, presented in an increasing order of structural complexity. In section 4.4, more complex anions (derivitized benzenes and derivatized imides) are examined. In section 5, DFT computations are used to rationalize some of the findings, and the results are summarized and generalized in section 6. Due to the large amount of data, some spectra and tables are placed in the Supporting Information and are designated with an "S" (such as Figure 1S).

3. EXPERIMENTAL AND COMPUTATIONAL METHODS

3.1. Materials. Ionic liquids and related solids were obtained from Aldrich (with the exception of tetracyanoborate liquids that were obtained from Merck) and dried in a vacuum oven at 80 °C for 10−20 h prior to use. Their chemical compositions were verified using ^{1}H and ^{13}C nuclear magnetic resonance (NMR) on a 500 MHz Bruker Avance 3 spectrometer. The samples were handled in a nitrogen-filled glovebox. For the designation of ammonium and phosphonium cations, we follow the convention that the lengths of the normal alkyl chains are indicated following the symbol of the heteroatom, so that tri(hexyl)tetradecyl phosphonium is designated $P_{666,14}^+$ and Aliquat-336 (methyltri(capryl/octyl)ammonium) is designated N_{1888}^+. Some of the commercially obtained ILs were contaminated with a halide impurity; e.g., in a sample of C_{10}mim BF_4 obtained from Aldrich, the $Br_2^{-\bullet}$ radical was quite prominent.

Some imidazolium compounds were H/D exchanged in their 2- and 4,5-positions in the ring (Scheme 1). The general procedure involved refluxing a 1−5 wt % solution of the IL in D_2O or a 3:1 v/v D_2O:acetonitrile mixture for 1−3 days, followed by removal of solvent at 80 °C, 25 mm Hg, and drying of the recovered liquid at 80−100 °C in a vacuum oven. The extent of the exchange was established using ^{1}H NMR. The protons in the aliphatic arms are not exchanged during this treatment. In the following, d_3 stands for H(2,4,5) deuterio substitution.

Several ILs were synthesized at Brookhaven National Laboratory using methods similar to those described in ref 41. For the synthesis of benzoates, salicylates, phthalimides, and perfluoro carboxylates and sulfates, we adapted the method of ref 42. Methylene chloride or chloroform solutions of $P_{666,14}^+$ or N_{1888}^+ chloride were stirred for 2 h with an aqueous inorganic salt solution to allow ion exchange. The organic phase was then separated, and the procedure was repeated 2−3 times. The organic layer was evaporated to dryness, the oily residue was dried in vacuo, and the chemical composition was examined by ^{1}H and ^{13}C NMR. Not all such ILs exchanged the chloride anion completely, but the chloride impurity does not produce observable radicals (section 4.1).

3.2. Spectroscopy. Liquid samples were degassed in a few freeze−thaw cycles and then frozen by rapid immersion into liquid N_2. Most of the ILs formed clear, transparent glasses. Some of the ILs were waxy, viscous liquids; these were heated to 50−60 °C in vacuo and rapidly quenched in liquid nitrogen before irradiation. Crystalline solids were evacuated for 15−30 min at room temperature.

Samples were placed in 4 mm diameter Suprasil tubes and irradiated at 77 K using 55 ns pulses of 3 MeV electrons from a Van de Graaff accelerator at Argonne. The typical dose was 1−3 kGy and the average electron current at the target was 1 μA. Following irradiation, samples were transferred into the resonator of a 9.45 GHz Bruker ESP300E spectrometer equipped with an Oxford Instruments CF935 cryostat. The modulation frequency was 100 kHz. The magnetic field and hyperfine coupling constants (hfcc's) are given in the units of Gauss (1 G = 10^{-4} T). First-derivative EPR spectra were obtained at several temperatures (the default temperature was 50 K), microwave power levels (2 μW and 2 mW), and modulation fields (2−5 G). Second-derivative spectra were obtained by numerical differentiation of these first-derivative EPR spectra. Relative radical abundances were estimated by numerical integration of these EPR spectra or comparisons of selected resonance lines with the simulated EPR spectra. Some radicals, especially aromatic and fluorinated ones, have long relaxation times at low temperatures, and care needs be exerted to avoid microwave saturation of their EPR signals.[14]

The irradiated samples were slowly warmed in the cryostat to the point of glass softening (200−250 K); some waxy and crystalline samples yielded radicals that persisted to 300−350 K. This warming has several effects: the radicals become mobile, react or undergo rearrangements and fragmentation, and recombine. In general, radicals derived from the anions decay at lower temperatures than the radicals derived from the cations. As the frozen ILs are fairly rigid matrices, these matrices hinder bond rotation of groups, which results in large magnetic anisotropy and poor rotational averaging. This rotation becomes free at a higher temperature (e.g., see Figure 12S(b) in section 4.3). Such reversible effects can be recognized by cycling the temperature.

Electron beam irradiation of Suprasil sample tubes yields H atoms that are trapped in the SiO_2:OH glass; these H atoms reveal themselves as a ∼500 G doublet of narrow lines superimposed on the EPR spectra from the sample. These EPR lines are not shown in the figures below; a narrow signal from E'_γ defect (silicon dangling bond) at $g \approx 1.99$ has also been removed from most of the EPR spectra (if the latter signal was not in saturation, which is frequently the case, given its extremely slow longitudinal relaxation).

As the EPR spectra of irradiated ILs are quite complex, with multiple overlapping lines from different radicals, it was necessary to examine reference systems of the corresponding alkali salts. In other cases, we needed to examine radicals that originate specifically from reaction 1a without other radiolytically induced reactions occurring in the ILs. To this end, aqueous solutions of the alkali salts were mixed with a pH = 3 solution of 2 nm anatase nanoparticles,[43] the solutions were flash frozen and then irradiated using 10 mJ, 6 ns pulses of 355 nm light from a Nd:YAG

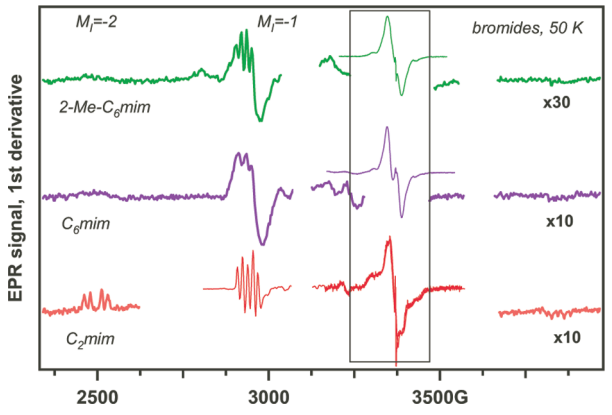

Figure 1. EPR spectra of irradiated crystalline 1-methyl-3-ethylimidazolium bromide and flash-frozen 1-methyl-3-hexyl- and 1,2-dimethyl-3-hexylimidazolium bromides. The spectra were obtained at 9.46 GHz and 50 K; the samples were irradiated at 77 K. The resonance lines in the box are from cation-derived organic radicals, the magnified lines are from the $Br_2^{-\bullet}$ radical anion (the $M_I = -1$ and -2 lines; see also Figure 1S, Supporting Information).

laser. The photoirradiated samples exhibit the typical EPR spectra for this oxide[43] that include a narrow line at $g \approx 1.97$ from lattice-trapped electrons ($Ti^{3+\bullet}$ ions) in the nanoparticle interior, a broad line at $g \approx 1.93$ from surface-trapped electrons, and a $g > 2.01$ signal from organic radicals generated through the oxidation of chemisorbed anions by the oxygen hole centers ($\equiv Ti^{4+}O^{\bullet}$ radicals) at the surface.

3.3. Calculations. Calculations of geometry and magnetic parameters were carried out using density functional theory (DFT) with the B3LYP functional[44] and 6-31+G(d,p) basis set from Gaussian 98.[45] In the following, *a* denotes the isotropic hfcc and *B* denotes the principal values of **B**, that is, the anisotropic part of the hfc tensor **A** (these tensors are mostly axial). Simulations of EPR spectra were carried out using first-order perturbation theory assuming a spherical *g* -tensor.

4. RESULTS

4.1. Halides and Dicyanamide. The formation and reactivity of $Br_2^{-\bullet}$ in N_{1444} NTf_2 was reported by Grodkowski, Neta, Marcinek, and their co-workers, who monitored this species through its typical optical absorption at 365 nm.[46,47] We have observed this radical anion in all of our irradiated bromides, both aliphatic (e.g., Figure 1S, Supporting Information) and aromatic (Figure 1). Since both ^{79}Br and ^{81}Br spin-3/2 nuclei are present in approximately equal natural abundances and the *g*- and hfcc-tensors are axial (Table 1S, Supporting Information), the EPR spectrum is rather complex, but it is immediately recognizable as a variant of the V_K centers observed in alkali halide crystals, such as NH_4Br (the comparison with the latter center, using magnetic parameters given in Table 1S, is shown in Figure 1S, Supporting Information). In particular, there is the characteristic 1:2:1 structure in the outermost $M_I = \pm 3$ lines from the isotopomers of $Br_2^{-\bullet}$ (as ^{81}Br has 8% greater magnetic moment than ^{79}Br, the line is split in a triplet; see Figure 1S, Supporting Information). In frozen (liquid) C_6mim Br and waxy 2-Me-C_6mim Br, the resonance lines of $Br_2^{-\bullet}$ are broad (Figure 1), but in crystalline C_2mim Br, these lines are well-resolved (Figure 1). Upon warming of the irradiated C_6mim Br, the resonance lines of $Br_2^{-\bullet}$ gradually become weaker as compared to the signal from the organic radicals ($Q_2H^{\bullet}$ and $Q_2H_2^{+\bullet}$, see Scheme 1) at $g \approx 2$. As the resonance signals from these radicals do not spectrally overlap with the resonance lines from $Br_2^{-\bullet}$ due to large differences in the *g*-factors, one can integrate both of these groups of EPR lines and demonstrate the approximate ($\pm$ 10%) parity between the yields of the $Br_2^{-\bullet}$ radical anions (that are derived from hole trapping by the bromide anion) and 2-imidazolyl radicals that are derived from electron trapping by the cations. The simultaneous disappearance of $Q_2H^{\bullet}$ and $Br_2^{-\bullet}$ at 170 K suggests that these trapped-charge species decay by back recombination. In waxy 2-Me-C_6mim Br, where the diffusion of radicals is suppressed, the signal from $Br_2^{-\bullet}$ persists to 350 K. The latter species is also observed in crystalline $N_{111,16}$ Br (Figure 1S, Supporting Information). The integration of the signals from $Br_2^{-\bullet}$ and $R^{\bullet}(C^+)$ indicates parity between the radiolytic yields of these two classes of radicals.

In contrast to these bromides, no signal from $Cl_2^{-\bullet}$ was found in ILs and related systems composed of aliphatic or aromatic cations and the chloride anion (e.g., Figure 2S(a), Supporting Information), with the single exception of 1,3-di(isopropyl)-imidazolium chloride (Figure 3S, Supporting Information), where the $M_I = -2$ and $M_I = -1$ lines of $Cl_2^{-\bullet}$ with the characteristic structure resulting from $^{35}C-^{35}Cl$, $^{35}Cl-^{37}Cl$, and $^{37}Cl-^{37}Cl$ isotopomers is observed.

As the $X_2^{-\bullet}$ anions are produced via 3-electron, 2-center $\sigma^2\sigma^{*1}$ bonding of the halogen atom, $X^{\bullet}$ (resulting from electron detachment from the parent anion) to the halide anion, the yield of $X_2^{-\bullet}$ depends on the reactivity of the released $X^{\bullet}$ atoms toward the organic cations. The energies of the H−X bond change from 5.9 to 4.5 to 3.8 eV from F to Cl to Br.[48] As chlorine atoms abstract hydrogen from organic cations more readily than bromine atoms, nondetection of $Cl_2^{-\bullet}$ is accounted for by the competition between the hydrogen abstraction and $\sigma\sigma^*$-bonding to the parent anion.

For ILs that contain such anions as Cl^-, ClO_4^-, BF_4^-, and PF_6^-, only organic radicals derived from the cation are observed. For PF_6^- and BF_4^-, mass-spectrometry analyses indicate the occurrence of $F^{\bullet}$ atom substitution/addition products,[29,31] whereas EPR indicates no anion-derived radicals that are stable at 50 K. Since the irradiation of KPF_6 and KBF_4 definitely yields P- and B-centered radicals (shown in Figure 4S, Supporting Information), the absence of anion-derived radicals in the corresponding ILs (e.g., Figure 2S(b), Supporting Information) suggests that $F^{\bullet}$ atoms promptly react with the cations. When tetracyanoborate anion, $B(CN)_4^-$, replaces the BF_4^- anion, two B-centered anion-derived species are observed in the EPR spectra: the $B(CN)_3^{-\bullet}$ radical anion and the $^{\bullet}B(CN)_2$ radical (for the latter, only $M_I(^{11}B) = \pm 3/2$ components were resolved; see Figure 2 and Figure 5S, Supporting Information). The identity of the latter species is supported by the agreement between the hfcc parameters estimated using DFT (for ^{11}B, a = 79 G and $B_{||}$ = 23.6 G) and the experimental values (78 and 17.3 G, respectively; the contribution from the ^{10}B isotopomer of this radical is weak due to the low (20%) abundance of ^{10}B); see Figure 6S (Supporting Information) for spectrum simulation. The well-resolved lines from the $B(CN)_3^{-\bullet}$ anion are not observed in the presence of electron-scavenging additives (such as CD_2Cl_2) and both of these radicals are absent from the EPR spectra when 1,3-dinitrobenzene-d_4 (which reacts with the electrons and holes) is used as a scavenger. These observations suggest the following fragmentation

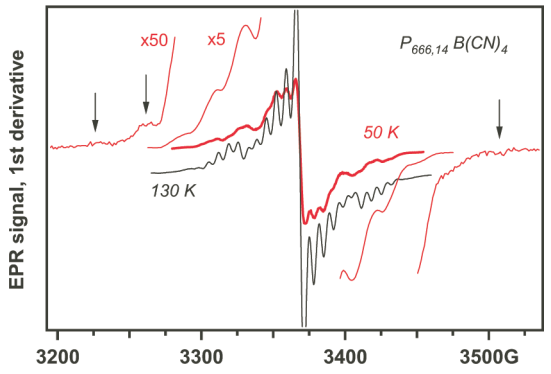

Figure 2. EPR spectra from irradiated $P_{666,14}$ tetracyanoborate. The wings in the 50 K spectrum are from the $^{\bullet}B(CN)_2$ radical (see the simulations in Figure 6S, Supporting Information), and the pattern of narrowly spaced lines are from the $B(CN)_3^{-\bullet}$ radical anion. These lines are fully resolved at 130 K.

pathways:

$$B(CN)_4^- + e^{-\bullet} \rightarrow B(CN)_3^- + CN^- \quad (2)$$

$$B(CN)_4^- + h^{+\bullet} \rightarrow {}^{\bullet}B(CN)_2 + C_2N_2 \quad (3)$$

The corresponding reactions involving BF_4^- do not occur. These observations are rationalized in section 5.

The chlorides, tetrafluoroborates, and perchlorates of N_{4444} all gave very similar EPR spectra dominated by the corresponding $R^{\bullet}(C^+)$ radical (Figure 2S(b), Supporting Information). Conversely, irradiated N_{1888} and $P_{666,14}$ chlorides gave similar EPR spectra despite the differences in the cation structure (Figure 2S(a), Supporting Information). In such aliphatic ILs, the main radiolytic products are penultimate and terminal H loss from the long arms of the onium cations.[14] If the alkyl chains are long, the EPR spectra are not particularly sensitive to the nature of the cation. For smaller aliphatic cations (such N_{2222}^+), the EPR spectra are quite different from those shown in Figure 3S (Supporting Information, not shown) as the $R^{\bullet}(C^+)$ radicals are strongly coupled to the central ^{14}N nucleus. We conclude that the released $Cl^{\bullet}$ or $F^{\bullet}$ atoms abstract H primarily from the extremities of the extended aliphatic chains.

One of the typical inorganic anions used for synthesis of hydrophobic ILs is dicyanamide, $N(CN)_2^-$. EPR spectra obtained in imidazolium dicyanamides are shown in Figure 7S(a) (Supporting Information). As this anion is a pseudohalide, in ref 15 we speculated that the oxidized anion, which is a π-radical, forms a N–N $\sigma^2\sigma^{*1}$ bond with its parent anion when the two N 2p orbitals line up, yielding a C_2 symmetric radical anion. In Figure 7S(b) (Supporting Information), we compare the EPR spectra obtained in irradiated C_4mim N $(CN)_2$ with the simulated EPR spectra for the monomer radical, $^{\bullet}N(CN)_2$, and the dimeric radical anion (with the hfcc parameters given in Table 2S, Supporting Information). The first derivative EPR spectrum (Figure 7S(a), Supporting Information) is dominated by the structureless signal from the 2-imidazolyl radical; this signal is superimposed on a set of ten weaker lines separated by 10–14 G. Comparison with the simulated spectra for $CN^{\bullet}$, $N(CN)_2^{2-\bullet}$, $HN(CN)_2^{-\bullet}$, $^{\bullet}N(CN)_2$ and $[N(CN)_2]^{2-\bullet}$ centers (Table 2S, Supporting Information) suggests that only the latter two structures can account for the observed lines, and only the dimeric anion can account for the span of this spectrum and the number of resonance lines. It appears that N–N bond formation is indeed taking place in this IL.

4.2. Hydrogen Sulfate and Nitrate. An important specific case of an inorganic IL anion is hydrogen sulfate, as it exemplifies acidic functionality in the constituent anion. The irradiation of C_2mimHOSO$_3$ yields a strong EPR signal from the $Q_2H_2^{+\bullet}$ radical that overwhelms all other signals (Figure 8S, Supporting Information). This indicates either the copious production of $H^{\bullet}$ atoms via

$$HOSO_3^- + e^{-\bullet} \rightarrow H^{\bullet} + SO_4^{2-} \quad (4)$$

resulting in the addition of the released hydrogen atoms to the C(2) atom in the imidazolium ring:

$$Q_2H^+ + H^{\bullet} \rightarrow Q_2H_2^{+\bullet} \quad (5)$$

or the ease of protonation of the 2-imidazolyl radical generated from the excess electron,

$$Q_2H^+ + e^{-\bullet} \rightarrow Q_2H^{\bullet} \quad (6)$$

$$Q_2H^{\bullet} + H^+ \rightarrow Q_2H_2^{+\bullet} \quad (7)$$

Another inorganic anion of great interest is nitrate, as nuclear separations typically involve nitric acid solutions. Accordingly, Allen et al. previously studied the γ and electron radiolysis of C_4mim NO_3 and noted transients that absorb in the visible, but disappear in less than 4 ms, and the accumulation of nitrite ion.[49a] We observe that irradiation of flash-frozen molten C_2mim NO_3 yields a complex EPR pattern, suggesting the presence of large crystallites and poor orientational averaging. To obtain a disordered solid, we mixed this IL with C_2mim BF_4 (1:1 w/w). The EPR spectrum obtained in this glassy solid (Figure 3a) can be compared with the one observed in polycrystalline KNO_3. The latter EPR spectrum is known to be mainly from $NO_3^{2-\bullet}$, $NO_2^{\bullet}$, and $NO_3^{\bullet}$ radicals resulting from electron attachment, excited state dissociation, and oxidation of the nitrate, respectively.[49b] The predominant lines in both of these solids are from the $NO_2^{\bullet}$ and $NO_3^{2-\bullet}$ radicals. The central resonance line for KNO_3 (Figure 3a) also reveals the 3.5 G pattern of the $NO_3^{\bullet}$ radical (Table 1S, Supporting Information). This pattern is lacking in the IL mixture. For comparison, we also irradiated polycrystalline N_{4444} NO_3 (Figure 3b). The $NO_3^{\bullet}$ radical was also missing in this solid. Due to the strong spectral overlap with the $NO_3^{2-\bullet}$ radical, only the z-components (with $g_{zz} \approx 1.995$ and $A_{zz} \approx 46.5$ G for the ^{14}N nucleus, Table 1S, Supporting Information) of the $NO_2^{\bullet}$ radical were observed. The spin parameters for the major radical (with axially symmetrical g- and $A[^{14}N]$-tensors: $g_{\perp} \approx 2.0073$, $A_{\perp} \approx 30.8$ G and $g_{\parallel} \approx 2.0010$, $A_{\parallel} \approx 65$ G) are close to those reported in the literature for the $NO_3^{2-\bullet}$ dianion (Table 1S, Supporting Information).

In both aliphatic and aromatic nitrates, the radicals derived from the organic cation are missing. In aqueous solutions, the $NO_2^{\bullet}$ radicals form not only via the prompt dissociation of the excited nitrate anion but also via a slower reaction of $NO_3^{2-\bullet}$ (or its protonated form, $HNO_3^{-\bullet}$) with acids, HB (including water), yielding the corresponding oxide anion as a byproduct:[49b,c]

$$NO_3^- + e^{-\bullet} \rightarrow NO_3^{2-\bullet} \quad (8)$$

$$NO_3^{2-\bullet} + 2HB \rightarrow NO_2^{\bullet} + H_2O + 2B^- \quad (9)$$

The $NO_3^{2-\bullet}$ is readily protonated by weak acids (such as alcohols and boric acid), and we speculate that the $NO_2^{\bullet}$ radicals

dx.doi.org/10.1021/jp2003062 |J. Phys. Chem. B 2011, 115, 3872–3888

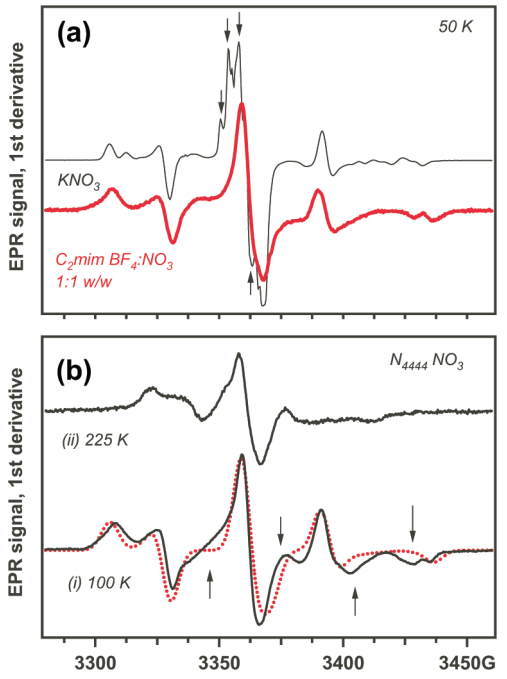

Figure 3. (a) EPR spectra from irradiated polycrystalline potassium nitrate (thin line) and 1:1 w/w mixture of aromatic ILs, 1-methyl-3-ethylimidazolium nitrate and tetrafluoroborate. The lines from the $NO_3^{\bullet}$ radical are present in KNO_3 but not in the ILs. Both spectra are dominated by the resonance lines from the $NO_3^{2-\bullet}$ radical dianion (or its protonated form). (b) Panel (i): EPR spectrum from irradiated crystalline tetrabutylammonium nitrate (50 K). The solid line is the experimental spectrum and the dashed line is the simulation for the $NO_3^{2-\bullet}$ radical with the parameters given in the text. The lines indicate the overlapping resonance signals from $NO_2^{\bullet}$ (see Table 1S (Supporting Information) for the parameters). The upper trace is the EPR spectrum observed at 225 K. This spectrum is from a radical whose magnetic parameters (given in the text) are consistent with those reported for $NO_2^{2-\bullet}$ or its protonated form (Table 1S, Supporting Information).

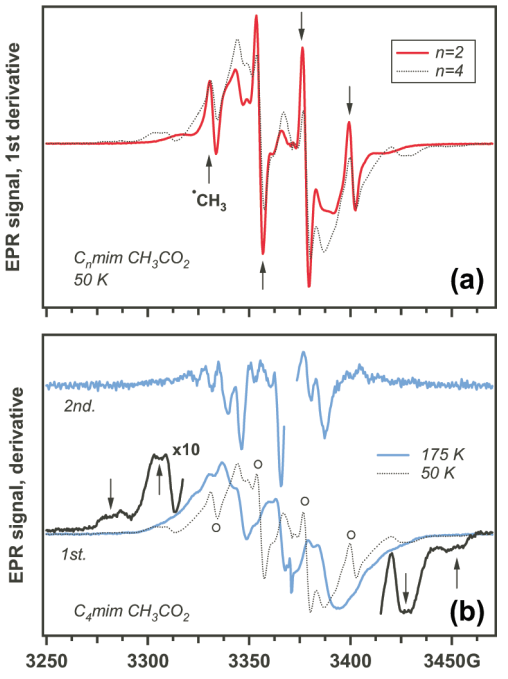

Figure 4. (a) EPR spectra obtained from irradiated 1-ethyl and 1-butyl-3-methylimidazolium acetate, $C_n$mim CH_3CO_2 ($n = 2$ and $n = 4$; see the legend). The four narrow lines indicated with arrows are from the methyl radical. (b) The spectra from the latter IL at 50 K (dashed line; the bold line shows the magnified spectral wings) and 175 K (solid line) when the methyl and $R^{\bullet}(C^+)$ radicals decay. The lines from the methyl radical are indicated with open circles and the lines from the $R^{\bullet}(C^+)$ radicals are indicated with arrows in the spectral wings. The upper curve is the second derivative of the 175 K trace. The 7 G pattern arises from the $Q_2HMe^{+\bullet}$ adduct radical cation.

observed in the ILs are generated in these secondary reactions. The $NO_2^{\bullet}$ radical can also be produced in reactions of $H^{\bullet}$ atoms and NO_3^-:[49c]

$$H^{\bullet} + NO_3^- \rightarrow NO_2^{\bullet} + HO^- \qquad (10)$$

When the N_{4444} NO_3 sample irradiated at 77 K is warmed to 225 K, the $NO_3^{2-\bullet}$ and $NO_2^{\bullet}$ radicals decay, and another N-centered radical with $g_{\perp} \approx 2.0079$, $A_{\perp} \approx 16.6$ G and $g_{\parallel} \approx 2.0037$, $A_{\parallel} \approx 43.5$ G is observed (the upper trace in Figure 3b). Among the known $NO_x^{\bullet}$ radicals, the $NO_2^{2-\bullet}$ radical anion provides the closest match (Table 1S, Supporting Information; note that this radical could also be in the protonated form, $HNO_2^{-\bullet}$). The formation of this radical could be due to electron transfer from $NO_3^{2-\bullet}$ to NO_2^-; the nitrite might be formed via the dissociation of the excited state NO_3^- anion. In C_2mim NO_3/BF_4, this $NO_2^{2-\bullet}$ radical is not observed; instead, at 175−180 K one observes a weak line resembling the resonance line of the superoxide radical.

We are presently unable to explain the low yield of the $NO_3^{\bullet}$ radicals in the irradiated ILs as compared to inorganic nitrate yields. In the aqueous solutions, the $NO_3^{\bullet}$ radicals decay by recombination with $NO_x^{\bullet}$ radicals or electron transfer from NO_2^-. $NO_3^{\bullet}$ also reacts with organic compounds, such as alcohols, amines, and imides, by H abstraction or electron transfer.[49c] The resulting hydrogen loss radicals recombine with $NO_3^{\bullet}$ radicals, forming organic nitrates (this reaction is well-known in atmospheric chemistry; see ref 50 for a review). Our observations of $NO_2^{\bullet}$ and $NO_2^{2-\bullet}$ radicals in the radiolysis of nitrate-containing ILs clearly indicate pathways for N−O scission leading to the production of nitrite ion observed by Allen et al.[49a]

4.3. Aliphatic RB^- Anions. The simplest of the RB^- anions (section 2) is acetate. Previous studies demonstrated that photocatalytic oxidation of acetate on TiO_2 yields the methyl radical exclusively, whereas the same reaction on the less oxidizing iron(III) oxides also yields $^{\bullet}CH_2CO_2^-$.[43] In radiolysis of C_2mim- and C_4mim CH_3CO_2, the EPR spectrum recorded at 50 K (Figure 4a) exhibits a quartet from the $^{\bullet}CH_3$ radical superimposed on the broad lines from 2-imidazolyl and $R^{\bullet}(C^+)$ radicals (the lines of the latter are indicated with arrows in Figure 4b and Figure 9S (Supporting Information) and compared to those observed in an aliphatic IL in Figure 9S(b), Supporting Information). The high yield of the latter species suggests that the released methyl radicals can abstract hydrogen from the aliphatic arms of the cation. At 175 K, the methyl radical disappears from the EPR spectra and a broad EPR signal shown in Figure 4b becomes prevalent. The second derivative EPR spectrum reveals the 7 G pattern of the $Q_2H_2^{+\bullet}$ or $Q_2HR'^{+\bullet}$ cations (the hfcc for the substituting alkyl radicals R′ in these 2-adducts are negligible,[16,33] so the nature of the substituting group other than H/D cannot be inferred from the EPR spectrum). The comparison with the analogous spectra for $Q_2H_2^{+\bullet}$ cations (see Figure 10S, Supporting Information, for the typical EPR spectra) indicates that this adduct is of the

dx.doi.org/10.1021/jp2003062 |J. Phys. Chem. B 2011, 115, 3872–3888

$Q_2HR'^{+\bullet}$ type. When the sample irradiated at 77 K was stored at this temperature for 90 days, the methyl radical fully decayed, and the EPR spectrum was dominated by $^{\bullet}CH_2CO_2^-$ (or the $^{\bullet}CH_2CO_2H$ radical) generated when the methyl radical abstracted H from the parent anion (Figure 9S(a), Supporting Information), in addition to the lines from the $Q_2HMe^{+\bullet}$ cation. Thus, the methyl radical decays by (i) H abstraction from the long arms of the cation and (ii) the parent anion and (iii) by thermally activated addition to the cation.

We turn to the effect of fluoridation on the anion chemistry. When trifluoromethyl replaces the methyl in the acetate anion (Figure 11S(a), Supporting Information), the EPR spectrum changes considerably. The main feature is a signal from $^{\bullet}CF_2CO_2^-$ radical whose $M_I = 0$ line overlaps with the signal from $Q_2H^{\bullet}$ and $R^{\bullet}(C^+)$ (see Table 3S (Supporting Information) for magnetic parameters). In addition to this −F radical, there is a weaker signal from the $^{\bullet}CF_3$ radical; see Figure 11S(b) (Supporting Information) for simulations with the parameters given in Table 3S (Supporting Information). This radical decays at 100 K, whereas $^{\bullet}CF_2CO_2^-$ persists to 150 K. The likely origin of this $^{\bullet}CF_2CO_2^-$ radical is dissociative electron attachment (DEA) to the parent anion:

$$CF_3CO_2^- + e^{-\bullet} \rightarrow F^- + {}^{\bullet}CF_2CO_2^- \qquad (11)$$

which is facilitated by the high electron affinity of fluorinated compounds. In irradiated N_{1888} CF_3CO_2 and $P_{666,14}$ CF_3CO_2, the same $^{\bullet}CF_2CO_2^-$ radicals were observed.

We also studied the radiation stability of anions with long fluorinated aliphatic chains, as these are desirable for some applications where greater IL hydrophobicity is required. To this end, ILs composed of the $CF_3CF_2CO_2^-$ anion were studied. In the crystalline sodium salt, the EPR spectrum revealed resonance lines from the $CF_3{}^{\bullet}CFCO_2^-$ and $^{\bullet}CF_2CF_2CO_2^-$ radicals generated via DEA (Figures 12S(a) and 13S, Supporting Information). The outermost lines from the $^{\bullet}CF_3CF_2$ radical generated via reaction (1) were also observed. Above 165 K, the $^{\bullet}CF_3CF_2$ radical decayed and the $^{\bullet}CF_2CF_2CO_2^-$ radical underwent a 1,2-shift to a more stable interior radical, $CF_3{}^{\bullet}CFCO_2^-$ (Figure 12S(b), Supporting Information). The well-resolved lines of the latter radical (indicative of a freely rotating trifluoromethyl group) can be observed without interference from other radicals at 225 K. Cooling of the sample hinders this rotation and the resulting EPR spectrum strongly resembles that observed in the sample before warming (Figure 12S(b), Supporting Information). In N_{1888} and $P_{666,14}$ $CF_3CF_2CO_2$ (Figure 14S(a), Supporting Information), only the $CF_3{}^{\bullet}CFCO_2^-$ and $^{\bullet}CF_2CF_2CO_2^-$ radicals were observed (there is no evidence for reaction 1a1 occurring), and the thermal evolution of the EPR spectrum is similar to that observed in the sodium salt (Figure 14S(b), Supporting Information). While the suppression of reaction 1a could be explained by the chloride impurity competing for the holes, it seems that DEA is the main reaction pathway for perfluorinated carboxylates. This propensity (and the generation of F^-) would limit the usefulness of such anions for applications in high radiation fields. As observed above, aliphatic carboxylates have similar limitations due to the ease of reaction 1b.

This behavior is not only specific to carboxylates: aliphatic sulfonates and sulfates exhibit similar chemistries. Radiolysis of crystalline CH_3OSO_3Na (Figure 15S(a), Supporting Information) yields a signal attributable to $^{\bullet}CH_2\sim$ radicals that

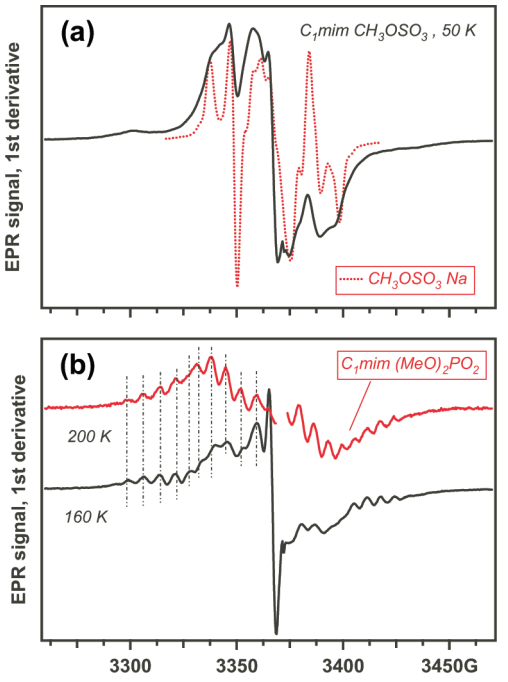

Figure 5. (a) EPR spectrum from irradiated frozen 1,3-dimethylimidazolium methyl sulfate, as observed at 50 K. For comparison, the spectrum of irradiated sodium methyl sulfate (dotted line) is superimposed on this trace. (b) EPR spectra for the same system at 160 K, where the lines from the $Q_2H(CH_2OH)^{+\bullet}$ adduct become fully resolved. For comparison, the 200 K spectrum of irradiated 1,3-dimethylimidazolium dimethyl phosphate is shown in the upper trace. Both spectra exhibit resonance lines from the same adduct radical cation.

can be either $^{\bullet}CH_2OSO_3^-$ (or its protonated form) or hydroxymethyl (from the internal rearrangement of the $CH_3O^{\bullet}$ radical generated in reaction 1b):

$$CH_3OSO_3^- + h^{+\bullet} \rightarrow \{CH_3OSO_3{}^{\bullet}\}^* \rightarrow {}^{\bullet}CH_2OH + SO_3 \text{ or } {}^{\bullet}CH_2OSO_3H \qquad (12)$$

Warming this sample to 180 K causes a characteristic change of the EPR spectrum (Figure 15S(a), Supporting Information) indicative of transformation of the methylene-terminated radical to another such radical, but with a lower coupling constant in the CH_2 protons; this would be consistent with the $^{\bullet}CH_2OH$ radical abstracting hydrogen from the parent anion. Above 100 K, the strongest EPR signal is a narrow line ascribed to the $CH_3OSO_3^{\bullet}$ radical; this resonance line persists to 300 K. It appears that the ground state $CH_3OSO_3^{\bullet}$ is very stable (which is in agreement with the estimates in Table 1), so reactions 12 should involve the excited state of this radical.

In the radiolysis of C_1mim CH_3OSO_3 (Figure 5a), the resonance lines from the $^{\bullet}CH_2\sim$ radicals are also present, but these lines strongly overlap lines from the $Q_2H^{\bullet}$ and $CH_3OSO_3^{\bullet}$ radicals. The narrow line of the latter radical is most distinctive in 2-Me-C_1mim CH_3OSO_3 (Figure 16S(a), Supporting Information). Above 125 K, these $^{\bullet}CH_2\sim$ radicals decay and $Q_2HR'^{+\bullet}$ cations form, suggesting that the released $^{\bullet}CH_2-$ radicals add to the C(2) atom of the cation (Figure 5b and Figure 16S(b), Supporting Information). The same C(2) adduct is observed (in the same temperature range) in irradiated $C_1mim(MeO)_2PO_2$ (Figure 5b), and this coincidence suggests that the $Q_2HR'^{+\bullet}$ adduct is of the $^{\bullet}CH_2OH$ radical. In addition to

dx.doi.org/10.1021/jp2003062 |J. Phys. Chem. B 2011, 115, 3872–3888

C_1mim $MeOSO_3$, we examined C_2mim $EtOSO_3$ (Figure 15S(b), Supporting Information). The EPR spectrum for this IL was dominated by the $CH_3^{\bullet}CHOH$ radical generated in reaction 12. In general, *the longer the aliphatic chain in the* RB^- *anion, the more extensive the fragmentation by deprotonation as compared to that by reaction* 1b.

We proceed to examine another popular choice for IL anions, viz. the dialkyl phosphates. Nelson and Symons[51a] have already studied radicals generated in the radiolysis of alkali salts of the dialkyl phosphates, $(RO)_2PO_2^-$, and observed significant yield of phosphoryl $ROPO_2^{-\bullet}$ and alkyl radicals (from electron trapping) and also some phosphoranyl $(RO)_2PO_2^{2-\bullet}$ radicals. In addition to these P-centered radicals, radicals arising from hydrogen loss in the alkyl arms were observed. Only the latter radicals were observed in photoionization of aqueous monoalkyl and dialkyl phosphates[51b] and γ-irradiated silver diethyl phosphate.[51c] The suggested mechanism for the formation of these radicals involves the formation of metastable $(RO)_2PO_2^{\bullet}$ radical via reaction 1a that either abstracts H atom from a neighboring $(RO)_2PO_2^-$ anion or undergoes the internal hydrogen abstraction (analogous to reaction 12).[51] The latter reaction can also be regarded as oxidative deprotonation.

None of these P-centered radicals and alkyl radicals[51a] were observed in irradiated $C_n$mim dialkyl phosphates; only the hydrogen loss radicals were generated, as in the other systems where electron attachment reactions were suppressed.[51b,c] Because the EPR spectrum of a $^{\bullet}CH_2\sim$ radical (which can be either the $^{\bullet}CH_2OH$ or $^{\bullet}CH_2O(CH_3O)PO_2^-$) strongly overlaps with that of the $Q_2H^{\bullet}$ radical, we synthesized the corresponding d_3 cation, which yields a narrower signal (Figure 6a), so that it does not overlap with the $M_I = \pm 1$ lines of the $^{\bullet}CH_2\sim$ radical. As the latter radical decays at 140−150 K, the lines of the Q_2H-$(CH_2\sim)^{+\bullet}$ adduct appear, suggesting a carbon-2 atom addition similar to the one in Figure 5b. This addition is apparent through the comparison of EPR spectra of the adduct radicals for h_3 and d_3 isotopomers (Figure 6a) as the latter spectrum is narrower due to the absence of the large hfcc in the 2-proton. The occurrence of this addition suggests a small radical, i.e., the hydroxymethyl. Furthermore, EPR spectra for the C(2)-adduct radicals observed in C_2mim $(EtO)_2PO_2$ and C_1mim $(MeO)_2PO_2$ are very similar, suggesting the same chemistry (Figure 6b). For the former IL, the lines from the $CH_3^{\bullet}CH\sim$ radical are superimposed on the doublet of $Q_2H^{\bullet}$. For C_2mim $(BuO)_2PO_2$, resolving all of these spectral components was impossible, but the resonance lines indicated with arrows in Figure 17S (Supporting Information) indicate that for these longer chain dialkyl phosphates, the deprotonation becomes the predominant fragmentation pathway, as these lines can only be from the interior H loss radicals in the butyl arms of the $(BuO)_2PO_2^-$ anion. These resonance lines are not observed for dimethyl and diethyl phosphates (Figure 6).

In addition to these aromatic ILs, we examined an aliphatic dialkyl phosphate, N_{1444} $(BuO)_2PO_2$ (not shown). Again, P-centered radicals derived from the anion were not found in this aliphatic IL, and the EPR spectrum was similar to that found in N_{4444} chlorides and tetrafluoroborates. This suggests that the oxidized anion primarily fragments by proton transfer, as in the previously studied systems,[51] yielding a radical whose EPR spectra is indistinguishable from the corresponding $R^{\bullet}(C^+)$ radicals.

The next representative class of the ILs anions includes alkyl sulfates and alkanesulfonates. The EPR spectra obtained by photooxidation of $CH_3SO_3^-$ and $CH_3OSO_3^-$ on TiO_2 look similar despite the structural differences between these anions

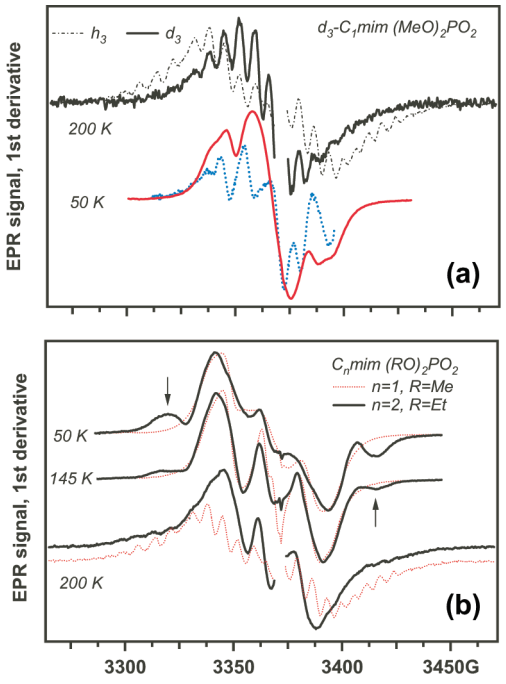

Figure 6. (a) Lower traces: the solid line is the EPR spectrum of irradiated 1,3-dimethylimidazolium-d_3(2,4,5) dimethyl phosphate observed at 50 K. Superimposed on this trace is the EPR spectrum (dotted line) of $^{\bullet}CH_2CO_2^-$ or $^{\bullet}CH_2CO_2H$ radicals observed in photolytic oxidation of malonate on hematite (irradiated by 355 nm light).[43] The upper trace is the EPR spectrum obtained at 200 K for the two isotopomers of the cation. (b) Comparison of EPR spectra for 1, 3-dimethylimidazolium dimethyl phosphate (dotted lines) and 1-methyl-3-ethylimidazolium diethyl phosphate (solid lines), as observed at 50, 145, and 200 K. The lines from the ethyl group derived radicals are indicated with arrows. In the 200 K trace, the resonance lines of the adduct radical cation are resolved in the wings.

(Figure 18S, Supporting Information); the predominant radicals observed for methyl sulfate being $^{\bullet}CH_2SO_3^-$ (or its protonated form) and $CH_3SO_3^{\bullet}$ (a narrow line at the center). The latter radical is the main oxidation product, suggesting the stability of this radical (in accord with the estimates given in Table 1). No methyl radical formation via reaction 1b was apparent. In contrast, electron irradiation of CH_3SO_3Na (Figure 19S, Supporting Information) produced the methyl radical in addition to these two radicals; $CH_3SO_3^{\bullet}$ comprises ≈10% of the total radical yield, while $^{\bullet}CH_3$ comprises ≈6% of the total radical yield. At 200 K, the methyl radical disappears while $^{\bullet}CH_2SO_3^-$ persists. The resonance lines from $^{\bullet}CH_2SO_3^-$, $CH_3SO_3^{\bullet}$, and $^{\bullet}CH_3$ are discernible in EPR spectra of irradiated N_{4444}- and P_{4444} CH_3SO_3 (Figure 19S(b), Supporting Information), where these lines are superimposed on the lines of $R^{\bullet}(C^+)$ radicals. In Figure 20S (Supporting Information) we compare EPR spectra obtained for C_2mim, C_4mim, and $NaCH_3SO_3$. In these spectra, the lines from the three principal radicals identified above are superimposed on a broad line from $Q_2H^{\bullet}$; the narrow line of the $CH_3SO_3^{\bullet}$ radical at $g \approx 2$ makes the most visible contribution. A closer examination of second-derivative EPR spectra reveals the presence of the $^{\bullet}CH_3$ and $^{\bullet}CH_2SO_3^-$ radicals, the latter making the largest contribution. Thus, deprotonation of the oxidized anion occurs both for methanesulfonate and methyl sulfate.

Above, we have compared aliphatic carboxylates and their perfluorinated analogs; the same comparison can be made for the

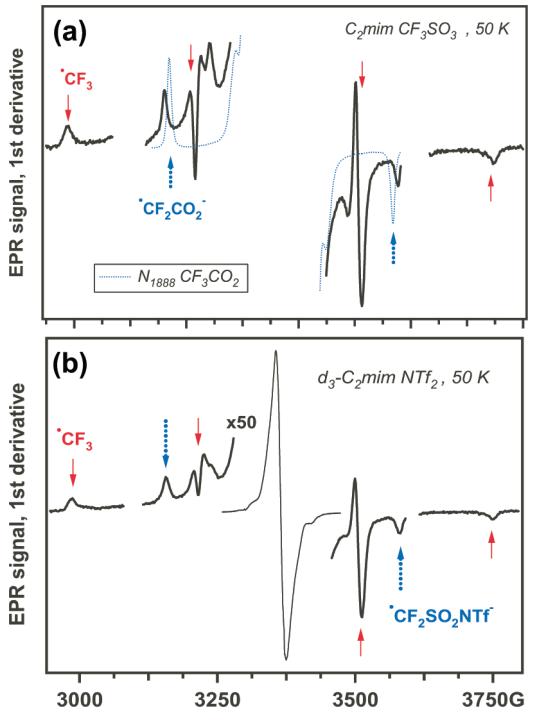

Figure 7. EPR spectra of irradiated (a) 1-methyl-3-ethylimidazolium triflate and (b) 1-methyl-3-ethylimidazolium-d_3(2,4,5) bistriflimide obtained at 50 K. In (a), the spectrum of the outer lines of the $^{\bullet}CF_2CO_2^-$ radical from irradiated 1-methyl-3-butylimidazolium trifluoroacetate (dotted line) is superimposed on the resonance lines from $^{\bullet}CF_2SO_3^-$ (indicated with dashed arrows). The resonance lines from the trifluoromethyl radical are indicated with solid arrows. In (b), dashed arrows indicate the resonance lines from −F loss radical resulting from dissociative electron attachment to the trifluoromethyl group of the bistriflimide anion.

alkyl sulfates and alkanesulfonates. One of these fluorinated anions, triflate, is a popular anion choice for IL synthesis. As exemplified in Figure 7a, radiolysis of $C_n$mim CF_3SO_3 yields two anion-related species, $^{\bullet}CF_3$ and $^{\bullet}CF_2SO_3^-$ (or its protonated form); the same two radicals were observed in irradiated CF_3SO_3Li (Figure 21S, Supporting Information). Unlike the case of $C_n$mim CF_3CO_2, where the $^{\bullet}CF_2CO_2^-$ radical accounts for most of the radicals observed, the yield of these two radicals in $C_n$mim CF_3CO_2 is low (<5% total); most of the EPR signal is from cation-related radicals. The same fragment radicals, $^{\bullet}CF_3$ and $^{\bullet}CF_2SO_3^-$ were also found in irradiated N_{2222}- and S_{222} CF_3SO_3, also with relatively low yield.

Interestingly, no evidence for the $CF_3SO_3^{\bullet}$ radical (analogous to the $CH_3OSO_3^{\bullet}$ and $CH_3SO_3^{\bullet}$ radicals observed in the reference ILs) was found in these triflate IL systems, suggesting that this radical is unstable. A literature review revealed no other reported observed instances of this radical, while its isomer, $CF_3OSO_2^{\bullet}$, has been observed.[52] The estimates for the C−S bond dissociation energies given in Table 1 suggest that the gas-phase C−S dissociation barrier for $CH_3SO_3^{\bullet}$ radical is considerably greater as compared to that for the $CF_3SO_3^{\bullet}$ radical (1.04 vs 0.3 eV), which may account for the instability of the latter species.

As ILs consisting of the exceptionally stable triflate anion are insufficiently hydrophobic for many applications, it is pertinent to consider long-chain perfluorinated sulfonates. Irradiation of n-$C_4F_9SO_3K$ yields a complex EPR spectrum arising from −F radicals (Figure 22S, Supporting Information). The EPR spectra for irradiated N_{1888} n-$C_4F_9SO_3$ shown in Figure 23S(a) (Supporting Information) yields broad, poorly resolved lines that persist to 200 K; very similar EPR spectra were obtained for irradiated N_{4444} n-$C_{17}F_{35}SO_3$ and N_{2222} n-$C_8F_{17}SO_3$ (Figure 23S(b), Supporting Information). In the center region of the spectra, the integrated EPR signals compare to the signals from the $R^{\bullet}(C^+)$ radicals, suggesting that these broad lines are from F^- loss radicals generated via DEA. The increased yield of the DEA in such ILs is attributed to two factors. First, the longer chain provides more sites for F^- loss. Second, the decreasing effect of the sulfate group (repelling the excess negative charge) results in more efficient electron trapping.

A closely related anion to the fluorinated sulfonates is bistriflimide, which is widely utilized due to its hydrophobicity. In a previous study, we identified two radicals derived from this anion: the $^{\bullet}NTf_2$ radical (which was resolved in tetraalkylammonium ILs) and the $^{\bullet}CF_3$ radical (that accounts for 2−5% of the total radical yield in irradiated bistriflimide ILs).[14] In light of the present results for triflate, we re-examined these ILs and realized that two sharp resonance lines that we attributed to $^{\bullet}CF_3$ (that could potentially arise from anisotropy alone) belong to a $^{\bullet}CF_2$∼ radical (Figure 7b). Therefore, in addition to oxidation (which results in the formation of an N-centered radical), bistriflimide undergoes DEA typical of other fluorinated anions, albeit with a small yield (comparable to the yield of the $^{\bullet}CF_3$ radical):

$$NTf_2^- + e^{-\bullet} \rightarrow F^- + {}^{\bullet}CF_2SO_2NTf^- \qquad (13)$$

The relative yields of $^{\bullet}CF_3$ and $^{\bullet}CF_2$∼, as compared to cation-derived radicals, are similar for both the TfO^- and NTf_2^- anions. There is another similarity: in triflate ILs, no $CF_3SO_3^{\bullet}$ radicals were observed. Likewise, in the bistriflimide ILs, no $CF_3SO_2^{\bullet}$ radical from the fragmentation of NTf_2^- was observed. The discussion of the bistriflimide fragmentation is continued in section 5.

4.4. Aromatic Anions. Given the propensity for RB^- anions to fragment (section 4.3), is it possible to stabilize such anions by π-conjugation? DFT calculations carried out in ref 43 for aromatic carboxylates suggest that reaction 1a is least exothermic for monocarboxylated benzenes, such as benzoic (**1** in Scheme 2) and (thio)salicylic acid (**2** and **3**). Indeed, the $PhCO_2^{\bullet}$ radical (**1a**) has been observed previously in the EPR studies (Table 2S, Supporting Information) suggesting its relative stability. The greatly decreased rate of decarboxylation of aroyloxyl radicals in room-temperature solutions is also known from laser photolysis studies of Ingold and coworkers;[40b] only few other carbonyloxyl radicals (such as alkenyl- and alykynyl-carbonyloxyls) have comparably slow decarboxylation rates, which makes the derivatives of the benzoic acid rather unique among organic acids.

The EPR spectrum observed for irradiated sodium benzoate exhibits a narrow line of radical **1a** (see Table 4S, Supporting Information). The same line is observed in irradiated $P_{666,14}$ benzoate (Figure 24S, Supporting Information) where it accounts for ≈20% of the total radical yield. This signal is superimposed on the spectrum from $R^{\bullet}(C^+)$ radicals and a weak signal (that is most clearly observed at 190 K), whose spectrum matches that of radical **1b**. No lines from radical **1c** formed in reaction 1b have been found. This is as much the effect of the energetics (Table 1) as the matrix; as in radiolysis of crystalline N_{4444} benzoate (Figure 8a), the lines of radical **1c** are superimposed

dx.doi.org/10.1021/jp2003062 |J. Phys. Chem. B 2011, 115, 3872–3888

Scheme 2. Fragmentation of Complex Anions (Section 4.4)

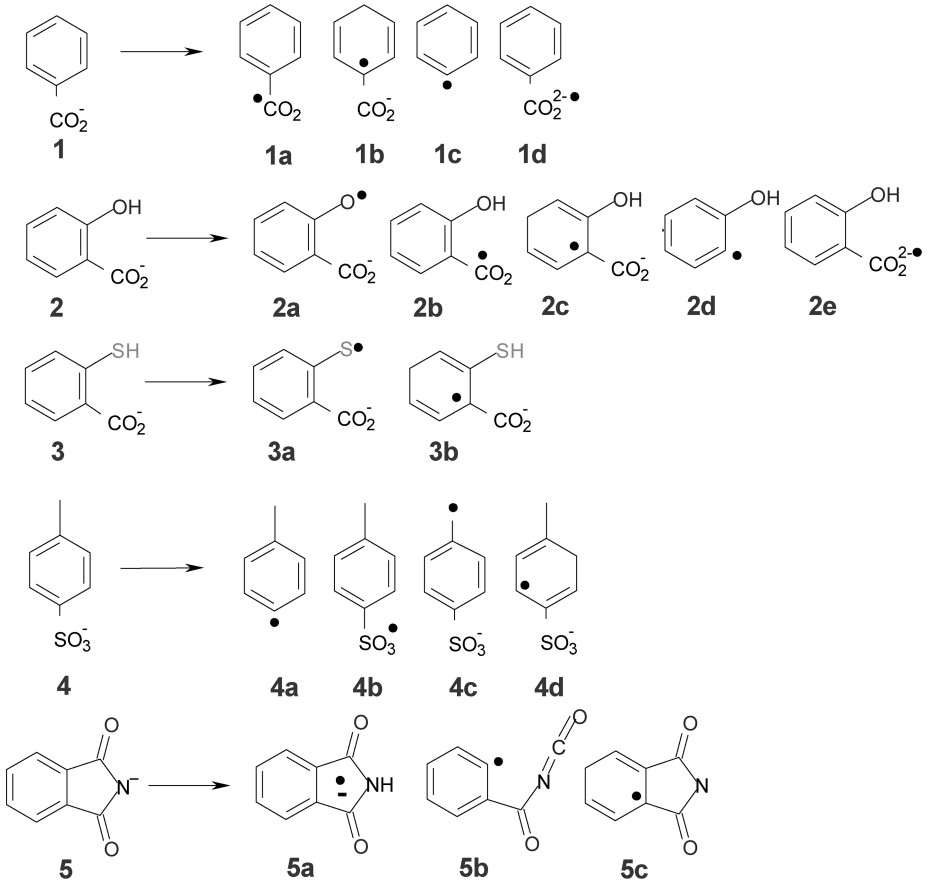

on the resonance line of radical **1a**. When the same material is quenched from a melt at 77 K, the EPR spectrum of the irradiated sample (Figure 8) exhibited a resonance line of radical **1d**. The latter species is known from previous studies, and its magnetic parameters match both reported values (Table 4S, Supporting Information) and our DFT calculations (Figure 8b). It appears that benzoate serves not only as a hole scavenger (yielding radical **1a**) but also as an electron and H-atom acceptor (yielding radicals **1d** and **1b**, respectively). *Neither one of these reaction pathways results in the fragmentation of the benzoate anion.*

The oxidation of salicylate (**2**) on aqueous TiO_2 (Figure 25S, Supporting Information) yields the phenoxy radical **2a** with a characteristic *g*-factor of 2.0048. The EPR spectrum of irradiated sodium salicylate (Figure 9a and Figure 25S, Supporting Information) shows three groups of resonance lines: (i) a narrow line from radical **2b**, (ii) the signal from radical **2a**, and (iii) a weak doublet of triplets that becomes fully resolved at 200 K (Figure 9b). Simulation of this EPR spectrum using the calculated parameters for H-atom adducts (Table 4S and Figure 25S, Supporting Information) suggests that it is radical **2c**. Apparently, oxidation of salicylate yields **2b**, which undergoes internal deprotonation (yielding radical **2a**) in aqueous media but is more stable in the IL. In irradiated $P_{666,14}$ salicylate (Figure 26S(a), Supporting Information), both of these radicals (**2a** and **2b**) are prominent, with radical **2b** accounting for 37% of the total radical yield (Figure 26S(b), Supporting Information). These signals are superimposed on resonance lines from $R^{\bullet}(C^{+})$. The phenoxy radical **2a** decays at 200 K while radical **2b** persists to 220 K (Figure 26S(b), Supporting Information); at intermediate temperatures, the narrow line of radical **2b** is superimposed on the weaker lines from radical **2c**. In contrast, the EPR spectrum of irradiated N_{1888} salicylate (Figure 9a and Figure 27S, Supporting Information) was dominated by radical **2a**, while radical **2b** was not observed (as is the case for aqueous TiO_2 solutions, Figure 25S, Supporting Information). Instead, we observed overlapping lines from radicals **2a**, **2c**, and **2d** (Figure 27S(b), Supporting Information); the latter radical is the product of reaction 1b. As radical **2a** has an EPR spectrum similar to that of radical **2e**, it is possible that the latter EPR signal originates from electron rather than hole reactions. When N_{1888} salicylate is exposed to an excess of salicylic acid (Figure 28S, Supporting Information), radical **2c** is the predominant feature of the EPR spectrum.

It can be expected that deprotonation from the sulfhydryl group in oxidized **3** would be more efficient than in **2**. Figure 9a exhibits the EPR spectrum observed in irradiated N_{1888} thiosalicylate. The main feature is the doublet of radical **3a** with $g \approx 2.011$ typical of S-centered radicals, including the S−S bound dimer radical ion (Table 4S, Supporting Information). The resonance lines of this radical are superimposed on weaker lines of $R^{\bullet}(C^{+})$ and, above 200 K, on the lines of radical **3b** (Figure 9b). There is no evidence for the occurrence of reaction 1b in this IL: oxidative decarboxylation is suppressed and fragmentation occurs by deprotonation, with the formation of relatively stable (thio)phenoxy radicals **2a** and **3a**. Given these

dx.doi.org/10.1021/jp2003062 |*J. Phys. Chem. B* 2011, 115, 3872–3888

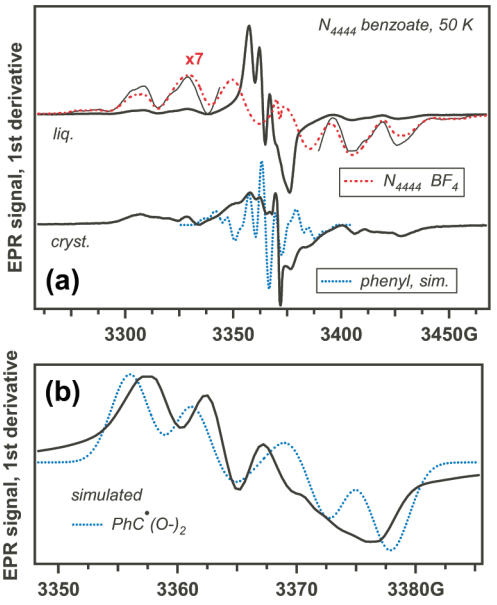

Figure 8. (a) EPR spectra observed from crystalline (lower trace) and flash-frozen molten tetrabutylammonium benzoate. In the lower trace, a simulated spectrum of the phenyl radical (dotted line) is superimposed on the experimental spectrum. In the upper trace, the spectrum of the $R^{\bullet}(C^{+})$ radical as observed in tetrabutylammonium tetrafluoroborate is superimposed on the wings of the spectrum from the tetrabutylammonium benzoate. The central feature in this spectrum (panel b) is from the radical dianion of benzoate, as suggested by the comparison with the simulated spectrum obtained using the magnetic parameters in Table 4S (Supporting Information).

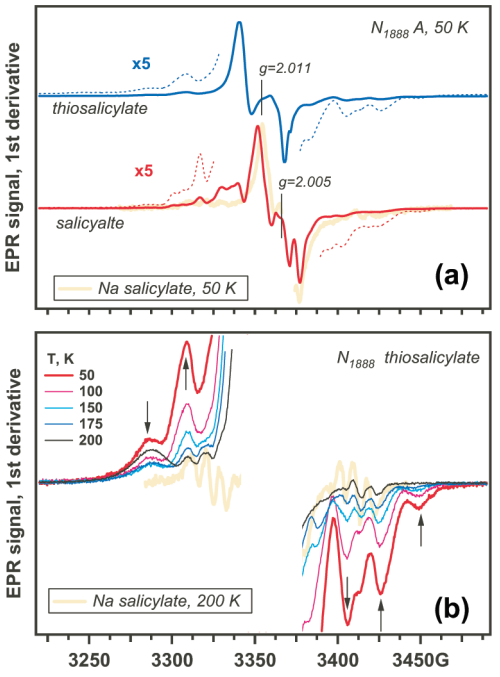

Figure 9. (a) Comparison of EPR spectra obtained from irradiated N_{1888} salicylate (lower trace) and thiosalicylate (upper trace). In the lower trace, the EPR spectrum from irradiated sodium salicylate is superimposed for comparison. The predominant EPR signal in both of these ILs is from the (thio)phenoxy radical. In (b), the wings of the EPR spectra obtained at different temperatures are shown for thiosalicylate. As the $R^{\bullet}(C^{+})$ radical (whose outer lines are indicated with arrows in the plot) decays at higher temperature, the triplets from H-atom adduct radical **3b** appear.

results, we speculate that sulfonated benzenes may also be stable, as Table 1 suggests that the C−S bond dissociation energy in arenesulfonates is higher than in the corresponding alkanesulfonates. However, photooxidation of tosylate **4** on aqueous TiO_2 (Figure 29S(a), Supporting Information) yields a poorly resolved EPR signal from radical **4a**, suggesting the occurrence of reaction 1b in the presence of water reacting with the released SO_3. For irradiated sodium tosylate, this radical was not observed; instead, there was a strong narrow line from radical **4b** (Figure 29S(b), Supporting Information) and weak signals from radical **4d**. In radiolyzed N_{1888}, P_{4444}, and methyl-(triisopropyl)phosphonium tosylates, this narrow line was absent (Figure 10 and Figure 30S(a), Supporting Information). Instead, superimposed on the signal from $R^{\bullet}(C^{+})$ radicals, there were overlapping lines of radicals **4a** and **4c** (Figure 10a and Table 4S, Supporting Information). At 170−225 K, the $R^{\bullet}(C^{+})$ radicals decay and the lines of radical **4d** become apparent (Figure 10b). In addition to these aliphatic ILs, we examined C_4mim tosylate. The EPR spectrum obtained at 50 K was mainly from $Q_2H^{\bullet}$. As the latter decayed at 220 K, the residual signal was identical to the ones observed in other tosylate ILs (Figure 30S(b), Supporting Information).

As both the dicyanamide (section 4.1) and bistriflimide (section 4.3) yield few radical fragments in radiolysis of their corresponding ILs, we conjecture that combining the $>N^{-}$ group with an aromatic π−system may yield hydrophobic anions that are resistant to radiolysis. Phthalimide (**5**) is the simplest such anion. It is known that oxidized aliphatic imides, such as succinimide, yield an N-centered π-radical that undergoes β-scission, yielding the corresponding alkyl radical (in this case, $^{\bullet}CH_2CH_2C(O)NCO$).[53,54] This rearrangement occurs above 20 K, so the parent radical has not been observed by EPR above 50 K;[53] in a room temperature aqueous solution, this ring-opening occurs on a millisecond time scale.[54] Irradiation of sodium phthalimide produced a complex EPR spectrum with a narrow line superimposed on two groups of weaker lines (not shown). From the known hfcc parameters for the phthalimide-derived radicals,[53] the narrow line can only be attributed to radical dianion or its protonated form radical **5a** (which is more likely due to high proton affinity of this dianion). These radicals are generated via reactions

$$R_2N^{-} + e^{-\bullet} \rightarrow R_2N^{2-\bullet} \quad (14)$$

$$R_2N^{2-\bullet} + H^{+} \rightarrow R_2NH^{-\bullet} \quad (15)$$

The weaker EPR signal can be interpreted as the superposition of the resonance lines from radicals **5b** (derived via ring-opening in the oxidized phthalimide) and **5c**. The EPR spectra for irradiated N_{1888} and $P_{666,14}$ phthalimides (Figure 11a) exhibit the same narrow line of radical **5a** that accounts for 35% and 20% of the total radical yield, respectively; the $R^{\bullet}(C^{+})$ contributes the remainder. This narrow signal persists at 225 K when the alkyl radicals decay. Above 150 K, there are also weak lines due to radical **5c** (Figure 11b). In these ILs, there is no evidence for the occurrence of ring-opening. Thus, the phthalimide anion in these ILs serves as an electron and H-atom scavenger rather than as a hole scavenger. Phthalimide provides another important example of a radiation resistant anion.

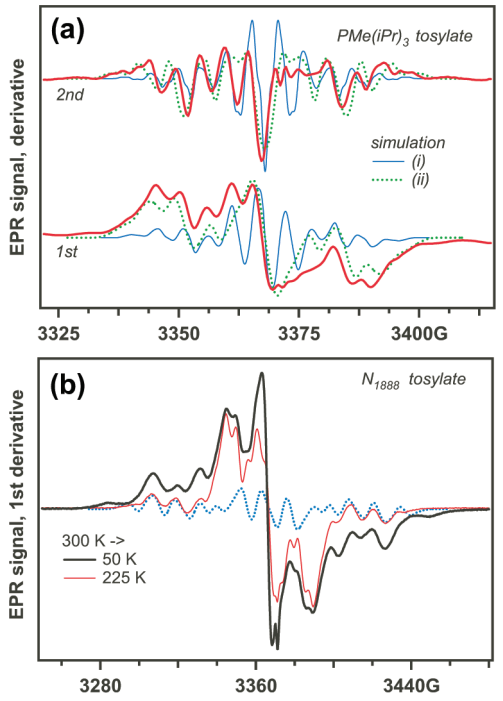

Figure 10. (a) First and second derivative EPR spectra obtained for irradiated methyl(triisopropyl)phosphonium tosylate (bold solid line). Superimposed are the simulated spectra for radicals (i) **4c** and (ii) **4a** in Scheme 2. (b) Spectra for the same system obtained from a sample warmed to 300 K and then cooled to 225 K (thin solid line) and 50 K (bold line). Superimposed on these traces is the simulated spectrum for **4d**. The simulation parameters are given in Table 4S, Supporting Information.

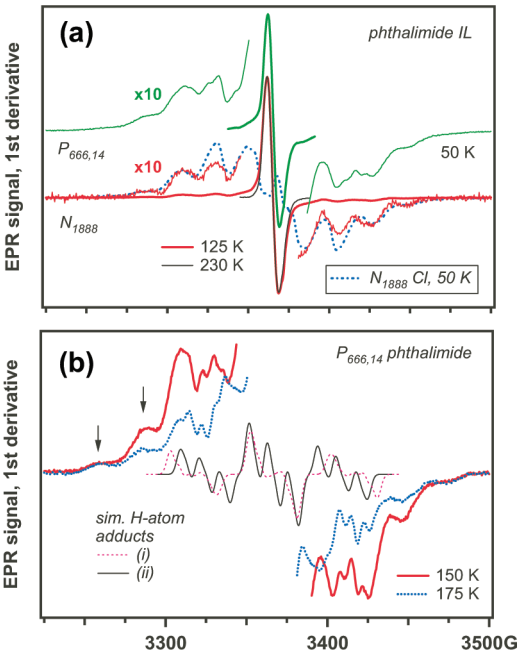

Figure 11. (a) EPR spectra obtained for irradiated $P_{666,14}$ and N_{1888} phthalimides. In both spectra, the narrow central lines are from the protonated radical dianion generated via electron attachment to the parent anion. The spectrum in the wings is from the $R^{\bullet}(C^{+})$ radical, as suggested by comparison with N_{1888} chloride (dot-dashed line in the lower trace). In (b), the spectral wings from $P_{666,14}$ phthalimide in the EPR spectra obtained at 150 K (bold solid line) and 175 K (bold dashed line) are shown. Superimposed on the broad lines from the $R^{\bullet}(C^{+})$ radical are the finer features from the H-adduct radical. The thin lines (see the legend) are simulated spectra for H-adducts in (i) 1- and (ii) 2-positions on the benzene ring of the phthalimide (see Table 4S (Supporting Information) for the simulation parameters).

We have examined one more imide system, N_{4444} succinimide (Figure 31S(a), Supporting Information). The EPR spectrum was cluttered, due to the strong overlap of the EPR signals from the anion-derived radicals and the $R^{\bullet}(C^{+})$ radicals, but the central feature in this EPR spectrum is consistent with the $>NH^{-\bullet}$ radical generated via reactions 14 and 15 (see simulations in Figure 31S(b), Supporting Information).

5. DISCUSSION

Generally speaking, damage to organic solvents (including ILs) is unavoidable during radiolysis: in a molecular system, the release of 10−20 eV of energy per excitation/ionization event cannot dissipate only as heat, without bond scission. The best that one can hope is for recombination of reactive intermediates before undergoing fragmentation and for dissipation of the excited state energy without extensive bond scission. If fragmentation occurs, as is usually the case, "radiation stability" signifies either the ability of these fragments to recombine and regenerate the parent molecules or an insignificant effect of accumulating fragments, where the products of their recombination do not affect the desired system performance. For example, "antirad" additives may convert the reactive fragment radicals to less reactive secondary radicals, thereby protecting the solvent from extensive damage.[55]

From this perspective, *improving the general radiation stability of ILs is a difficult task, as most short-lived reaction intermediates generated in radiolyzed ILs show a natural tendency to undergo rapid, irreversible reactions*. In particular, the constituent anions promptly deprotonate or undergo reaction 1b following oxidation. For fluorinated anions, F^{-} loss is equally facile. Such reactions result in the loss of functionality and the generation of acids. These ILs will inevitably accumulate damage in a radiation field; the question is whether the rate of accumulation is tolerable in the context of alternative processing systems.

However, the point is not to improve the generic radiation stability of all ILs but to identify radiation-stable classes of ILs for use in higher radiation fields. The extent of fragmentation greatly varies between ILs. The least stable anions are aliphatic carboxylates, arene- and alkanesulfonates, alkyl sulfates, and dialkyl phosphates, as well as their fluorinated derivatives. Among the fluorinated sulfonates, only the smallest anion, triflate, is relatively stable (section 4.3); longer chain anions are more easily defluorinated. Regrettably, these families of anions encompass many of the most popular types. The situation is similar for some small inorganic anions, such as nitrate or tetracyanoborate (section 4.1). Nevertheless, in section 4.4, we found two classes of anions that are exceptions to this general rule; it is possible that more such exceptions exist.

The first exception is the benzoate anion, which avoids decarboxylation due to the unusual stability of the corresponding radical **1a**. For its (thio)salicylate derivatives, the stability of the anion to oxidative decarboxylation is due to the occurrence of an internal proton transfer from the sulfhydryl or hydroxyl group. The latter reaction leads to the formation of (thio)phenoxy radicals **2a** and **3a** that are quite stable and unreactive toward the

constituent ions. This stabilization is a subtle effect: for example, the replacement of $-CO_2^-$ by an $-SO_3^-$ group leads to desulfonation (section 4.4). These "robust" anions do not react exclusively by hole scavenging; there is also electron trapping and H atom attachment, but the latter reactions do not result in *irreversible* structural damage.

The second exceptional class consists of imides. The apparent reason for their stability is that these pseudohalide anions do not belong to the RB^- class, so their radicals *cannot* undergo reaction 1b, in principle. The corresponding N-centered radicals appear to be unreactive toward the cations and so decay by back recombination, recovering the constituent anion. For dicyanamide, this N-centered radical undergoes additional stabilization via the formation of a $\sigma^2\sigma^{*1}$ bond to the parent anion (in analogy to $X_2^{-\bullet}$ dihalide anions). This dimeric radical anion was directly observed by EPR. For other imides, this dimer was not observed. For NTf_2^-, this N−N binding is unlikely due to steric hindrance,[15] but this hindrance also reduces the general reactivity of the $^\bullet NTf_2$ radical, achieving the same effect. For phthalimide, which is a planar and more accessible anion, the N−N bound dimer radical anion is known to occur in *N*-phthalimidophthalimide.[53] We have examined the N−N dimers for succinimide, maleimide, and phthalimide using DFT. The C_2 symmetric radical anions had the lowest energy, with the N−N bond length of ≈216 pm. The estimated binding energy was 1.02, 0.86, and 0.79 eV, respectively (Table 1). These binding energies compare favorably to 0.86 eV calculated for dicyanamide;[15] all of these energies are significantly lower than the binding energies for halides (Table 1). Nevertheless, as the N−N binding clearly occurs for the dicyanamide, it may also occur for these other imides, stabilizing their oxidized anions.

With matrix-isolation EPR, the radical species observed are the most stable ones: if the radical (ion) undergoes rapid back recombination, it cannot be observed, for obvious reasons. If the N-centered radical generated via the oxidation of these imide anions is intermediately stabilized via N−N dimer formation, this primes such a species to back recombination that competes with fragmentation. That there is some mechanism for stabilization of these radicals peculiar to the ILs is suggested by nonoccurrence of β-scission for the monomer radicals, which occurs for isolated radicals in low-temperature matrices[53] or dilute aqueous solution.[54] More indirect evidence for stabilization of oxidized imides and their efficient recombination is provided by mass-spectrometry studies of Moisy and co-workers,[29−31] as no inclusion/adduct products incorporating $-NTf_2$ functionality have been identified in radiolyzed bistriflimide ILs, suggesting that most of such radicals decay by back recombination.

While oxidative fragmentation is suppressed for these imides, this does not mean that these anions cannot react otherwise. Our EPR spectra suggest that phthalimide and succinimide trap the electron (reaction 14) and form H atom adducts. The bistriflimide anion also traps electrons, but due to the presence of trifluoromethyl groups it undergoes reaction 11. We also know from our EPR studies that the $^\bullet CF_3$ radical is produced while the $CF_3SO_2^\bullet$ radical was not observed. Mass-spectrometry data of Moisy and co-workers[29,30] suggest the occurrence of both N−S and S−C scission in the anion, as there are stable products, such as $(CF_3)_2SO_2$ and adducts of CF_3SO_2 and TfNH radicals, which can only be explained through the occurrence of this scission. While the $CH_3SO_2^\bullet$ radical is known from previous EPR studies,[56] the analogous $CF_3SO_2^\bullet$ radical has never been observed. According to our calculations (Table 1), the S−C dissociation energy for this radical is 0.26 eV, which is close to this energy for $CF_3SO_3^\bullet$ radical. The latter was not observed in radiolysis of triflate ILs (section 4.3). We suggest that the $CF_3SO_2^\bullet$ radical is unstable, even at the low temperature, as it undergoes reaction 1b similarly to the $CF_3SO_3^\bullet$ radical in the triflate ILs. Perhaps it is this reaction that accounts for radiolytic generation of sulfite reported in ref 28. To clarify the possible mechanism for the fragmentation of NTf_2^-, we estimated the energetics of dissociation pathways (Scheme 3).

Scheme 3. Energetics of Bistriflimide Dissociation

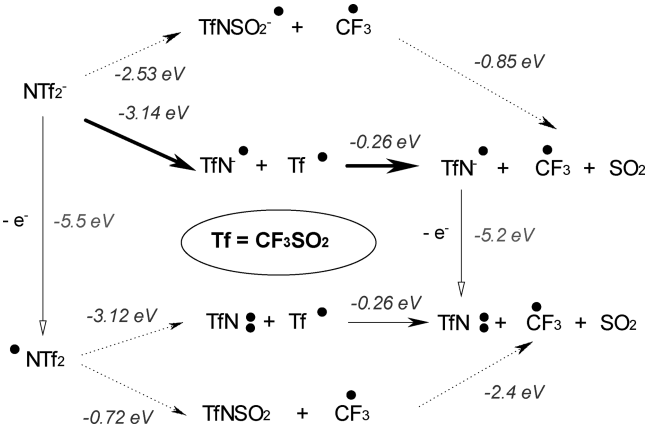

This dissociation can involve either the excited anion or electronically exited $^\bullet NTf_2$ radical. For the latter, there is a low-barrier $^\bullet CF_3 + TfNSO_2$ dissociation, whereas the dissociation to a nitrene $TfN^{\bullet\bullet}$ and $CF_3SO_2^\bullet$ requires >3 eV of the excitation energy. While the former reaction can account for generation of a $^\bullet CF_3$ radical, it does not account for the formation of sulfite[28] and the products derived from the (short-lived) $CF_3SO_2^\bullet$. For the excited NTf_2^- anion, the lowest energy channel is C−S dissociation to $^\bullet CF_3 + TfNSO_2^{-\bullet}$, but the N−C dissociation to a nitrene radical anion $TfN^{-\bullet}$ and $CF_3SO_2^\bullet$ is only 0.6 eV more energetic. Given the difference in size of the resulting radical anions, the difference in the polarization energy of the solvated species would be on the order of 0.5−1 eV; i.e., the N−C scission is likely to be preferred in the IL. The nitrene radical anion is known to abstract a proton from any organic molecule.[57] In imidazolium ILs, the C(2) proton is the most acidic.[16] The resulting imidazol-2-ylidene carbene $Q_2^{\bullet\bullet}$ should promptly react with the $TfNH^\bullet$ radical to produce $Q_2(N(H)Tf)^\bullet$ (the calculated proton affinity for $TfN^{-\bullet}$ is 13.3 eV vs 13 eV for NTf_2^- and 11.6 eV for $Q_2^{\bullet\bullet}$). Our calculations suggest that the overall reaction is exothermic by 1.5 eV. Indeed, mass spectrometry studies[31] indicate this $Q_2(N(H)Tf)^+$ adduct is one of the reaction products; the formation of the intermediate $TfN^{-\bullet}$ radical has already been postulated by Berthon et al.[31] By EPR spectrometry, distinguishing between the $^\bullet NTf_2$ and $TfN^{-\bullet}$ is impossible, as the two species have nearly identical hfcc's (Table 4S, Supporting Information), so the former radical would mask the resonance lines of the second should it be present in the irradiated IL.

Given these considerations, we suggest that the dissociation of NTf_2^- proceeds from the electronically excited state of the anion (which accounts for the relatively low yield of the fragment

dx.doi.org/10.1021/jp2003062 |J. Phys. Chem. B 2011, 115, 3872–3888

radicals) and involves the following three steps:

$$\{NTf_2^-\}^{**} \rightarrow TfN^{-\bullet} + CF_3SO_2^{\bullet} \quad (16)$$

$$CF_3SO_2^{\bullet} \rightarrow CF_3^{\bullet} + SO_2 \quad (17)$$

$$TfN^{-\bullet} + Q_2H^+ \rightarrow Q_2(N(H)Tf)^{\bullet} \quad (18)$$

where reaction 17 results in the delayed formation of $^{\bullet}CF_3$ radicals. The latter reaction could be driven to the right side by the solvation of the released SO_2 either by the IL itself or by reaction with adventitious water in the IL. For other imides, no evidence for N−C bond scission in the excited state of the anion was obtained.

Apart from these two classes of the anions, only PF_6^- and BF_4^- anions yield no direct EPR evidence for anion fragmentation. Since mass spectrometry studies directly implicate $F^{\bullet}$ atom formation,[28,30] and our EPR results (section 4.1) indicate that $Cl^{\bullet}$ atoms are generally unstable in ILs, reacting with the constituent cations, we account for these observations by invoking the high reactivity of the released $F^{\bullet}$ atoms, which promptly abstract H from the aliphatic arms of the cations:

$$BF_4^- + h^{+\bullet} \rightarrow BF_3 + F^{\bullet} \quad (19)$$

$$F^{\bullet} + RH(C^+) \rightarrow HF + R^{\bullet}(C^+) \quad (20)$$

Why are there no reactions for BF_4^- analogous to reactions 2 and 3 for $B(CN)_4^-$ yielding stable B-centered radicals? Remarkably, these fragmentation patterns can be rationalized using simple energetics arguments. In the gas phase, BF_3 has near-zero or negative electron affinity.[58] Had the BF_3^- radical been formed via reaction 2, it would donate the electron to any acceptor, including Q_2H^+. Our estimates suggest that the electron affinity of BF_3 is only 0.38 eV, whereas the electron affinity of $B(CN)_3$ is significantly higher (3.4 eV). The gas-phase electron affinity of Q_2H^+ is 3.94 eV, so only $B(CN)_3^-$ anion would avoid transferring the negative charge to the cation. In other words, had reaction 2 occurred for BF_4^-, it would not yield the *stable* $BF_3^{-\bullet}$ anion in the IL. The same relates to PF_6^- (we estimate that the dissociation of $PF_6^{\bullet}$ to $PF_5 + F^{\bullet}$ is exothermic by 0.6 eV). Equally significant is nonobservation of the $^{\bullet}BF_2$ radical analogous to the $^{\bullet}B(CN)_2$ radical formed in reaction 3. The dissociation energy for F_2 (1.61 eV)[48] is considerably lower than this energy for C_2N_2 (5.78 eV).[59] According to our calculations, the $BX_3 + X^{\bullet}$ pathway is preferred to the $^{\bullet}BX_2 + X_2$ pathway by almost 5.7 eV for X = F, whereas the second pathway is preferred by 0.7 eV for X = CN. Therefore, while reaction 19 occurs for the tetrafluoroborate anions, reaction 3 is preferred for the tetracyanoborate anions.

6. CONCLUDING REMARKS

In this study, EPR spectroscopy was used to identify radical (ions) derived from the constituent anions in irradiated ILs of practical interest. Most of the observed species are generated in radiolytically induced redox reactions. Our study indicates extensive fragmentation of the constituent anions and points to reaction (1) as the general culprit, with proton transfer involving the aliphatic arms of RB^- anions being the competing fragmentation pathway. In imidazolium ILs, the released radicals frequently add to the C(2) position of the parent cation or abstract H from the aliphatic arms of the constituent ions. For fluorinated anions, F^- loss following the electron attachment is quite prominent. Extensive bond scission was observed in NO_3^- and $B(CN)_4^-$ anions and implicated for BF_4^- and PF_6^- anions. Among smaller anions, only $CF_3SO_3^-$ and $N(CN)_2^-$ are relatively stable.

Though we cannot offer general principles for choosing radiation-resistant anions, reaction 1b has exceptions. Among larger anions, benzoate and imide anions were found to be stable. This stability is due to the suppression of the oxidative fragmentation. For the imides, this stability could be due to N−N bond formation involving the parent anion. This 3-electron bonding fleetingly stabilizes the N-centered π-radical so that it recombines with its geminate partner, such as the 2-imidazolyl radical.

Oxidative fragmentation and other scission reactions result in the release of mobile, reactive fragment radicals (such as $^{\bullet}CF_3$, $^{\bullet}CH_2OH$, and $^{\bullet}CH_3$ radicals) and acid-forming oxides (such as SO_x). Among the commonly used constituent anions, aliphatic carboxylates are the least stable, followed by dialkyl phosphates and alkyl sulfates and alkanesulfonates. The imides (including dicyanamide) appear to be among the relatively stable constituent anions. Another class of ILs with improved radiation resistance includes (thio)salicylates (that are already being used in *d*-ion metal extractions).[42] While these anions undergo deprotonation, yielding (thio)phenoxy radicals, the latter are rather unreactive; so these anions serve as "antirads". The results of this survey suggest that ionic liquids containing the above-mentioned radiation-resistant anions should be systematically explored for applications involving radiation fields.

We emphasize that fragmentation of constituent anions represents only "half" of the encountered radiation damage in ionic liquids, as the constituent cations also undergo fragmentation. This chemistry is examined in Part 2 of this study.[33]

■ ASSOCIATED CONTENT

Supporting Information. Tables 1S−5S (isotropic hfcc's, corresponding tensors, *g*-factors, NMR data) and related references and Figures 1S−31S (EPR specrtra). This material is available free of charge via the Internet at http://pubs.acs.org.

■ AUTHOR INFORMATION

Corresponding Author

* E-mail: shkrob@anl.gov. Tel: (630) 252-9516.

■ ACKNOWLEDGMENT

We thank D. M. Bartels, R. A. Crowell, M. L. Dietz, D. C. Stepinski, E. W. Castner, Jr., and K. Takahashi for stimulating discussions, Dr. W. Pitner (Merck KGaA, Darmstadt) for donation of the tetracyanoborate ionic liquids used in this study, and Dr. Marie Thomas for the sample of C_6mimBr. The work at Argonne and Brookhaven was supported by the US-DOE Office of Science, Division of Chemical Sciences, Geosciences and Biosciences under contracts Nos. DE-AC02-06CH11357 and DE-AC02-98CH10886, respectively. The programmatic support via a DOE SISGR grant "An Integrated Basic Research Program for Advanced Nuclear Energy Separations Systems Based on Ionic Liquids" is gratefully acknowledged.

■ REFERENCES

(1) Plechkova, N. V.; Seddon, K. R. *Chem. Soc. Rev.* **2008**, *37*, 123–150.

(2) Wishart, J. F. *Energy Environ. Sci.* **2009**, *2*, 956–961.
(3) Hough, W. L.; Rogers, R. D. *Bull. Chem. Soc. Jpn.* **2007**, *80*, 2262–2269.
(4) Metlen, M. S. A.; Rogers, R. D. *Acc. Chem. Res.* **2007**, *40*, 1182–1192.
(5) Parvulescu, V. I.; Hardacre, C. *Chem. Rev.* **2007**, *107*, 2615–2665.
(6) Kato, N.; Higuchi, K.; Tanaka, H.; Nakajima, J.; Sano, T.; Toyoda, T. *Sol. Energy Mater. Sol. Cells* **2011**, *95*, 301–305.
(7) MacFarlane, D. R.; Pringle, J. M.; Howlett, P. C.; Forsyth, M. *Phys. Chem. Chem. Phys.* **2010**, *12*, 1659–1669.
(8) Zhou, F.; Liang, Y. M.; Liu, W. M. *Chem. Soc. Rev.* **2009**, *38*, 2590–2599.
(9) Tan, S. S. Y.; MacFarlane, D. R. In *Ionic Liquids*; Springer-Verlag Berlin: Berlin, 2009; Vol. 290, pp 311−339.
(10) Dietz, M. L.; Dzielawa, J. A.; Jensen, M. P.; Beitz, J. V.; Borkowski, M. In *Ionic Liquids IIIb: Fundamentals, Progress, Challenges and Opportunities: Transformations and Processes*; American Chemical Society: Washington, DC, 2005; Vol. 902, pp 2−18.
(11) Dietz, M. L. *Sep. Sci. Technol.* **2006**, *41*, 2047–2063.
(12) Han, X.; Armstrong, D. W. *Acc. Chem. Res.* **2007**, *40*, 1079–1086.
(13) Binnemans, K. *Chem. Rev.* **2007**, *107*, 2592–2614.
(14) Shkrob, I. A.; Chemerisov, S. D.; Wishart, J. F. *J. Phys. Chem. B* **2007**, *111*, 11786–11793.
(15) Shkrob, I. A.; Wishart, J. F. *J. Phys. Chem. B* **2009**, *113*, 5582–5592.
(16) Shkrob, I. A. *J. Phys. Chem. B* **2010**, *114*, 368–375.
(17) Nash, K. L. In *Separations for the Nuclear Fuel Cycle in the 21st Century*; Lumetta, G. J., Nash, K. L., Clark, S. B., Friese, J. I., Eds.; American Chemical Society: Washington, DC, 2006; Vol. 933, pp 21−40.
(18) Jensen, M. P.; Neuefeind, J.; Beitz, J. V.; Skanthakumar, S.; Soderholm, L. *J. Am. Chem. Soc.* **2003**, *125*, 15466–15473.
(19) Dietz, M. L.; Stepinski, D. C. *Talanta* **2008**, *75*, 598–603.
(20) Cocalia, V. A.; Gutowski, K. E.; Rogers, R. D. *Coord. Chem. Rev.* **2006**, *250*, 755–764.
(21) Cocalia, V. A.; Jensen, M. P.; Holbrey, J. D.; Spear, S. K.; Stepinski, D. C.; Rogers, R. D. *Dalton Trans.* **2005**, 1966–1971.
(22) Gaillard, C.; Moutiers, G.; Mariet, C.; Antoun, T.; Gadenne, B.; Hesemann, P.; Moreau, J. J. E.; Ouadi, A.; Labet, A.; Billard, I. In *Ionic Liquids IIIB: Fundamentals, Progress, Challenges and Opportunities: Transformations and Processes*; American Chemical Society: Washington, DC, 2005; Vol. 902, pp 19−32.
(23) Luo, H.; Dai, S.; Bonnesen, P. V.; Haverlock, T. J.; Moyer, B. A.; Buchanan, A. C. *Solvent Extr. Ion Exch.* **2006**, *24*, 19–31.
(24) Stepinski, D. C.; Vandegrift, G. F., III; Shkrob, I. A.; Wishart, J. F.; Kerr, K.; Dietz, M. L.; Qadah, D. T. D.; Garvey, S. L. *Ind. Eng. Chem. Res.* **2010**, *49*, 5863–5868.
(25) Chen, P. Y.; Hussey, C. L. *Electrochim. Acta* **2004**, *49*, 5125–5138.
(26) Yuan, L. Y.; Peng, J.; Xu, L.; Zhai, M. L.; Li, J. Q.; Wei, G. S. *J. Phys. Chem. B* **2009**, *113*, 8948–8952. Qi, M.; Wu, G.; Chen, S.; Liu, Y. *Radiat. Res.* **2007**, *167*, 508–514. Yuan, L. Y.; Peng, J.; Xu, L.; Zhai, M. L.; Li, J. Q.; Wei, G. S. *Radiat. Phys. Chem.* **2009**, *78*, 737–739.
(27) Yuan, L. Y.; Peng, J.; Xu, L.; Zhai, M. L.; Li, J. Q.; Wei, G. S. *Dalton Trans.* **2008**, 6358–6360.
(28) Yuan, L. Y.; Xu, C.; Peng, J.; Xu, L.; Zhai, M. L.; Li, J. Q.; Wei, G. S.; Shen, X. H. *Dalton Trans.* **2009**, 7873–7875.
(29) Berthon, L.; Nikitenko, S. I.; Bisel, I.; Berthon, C.; Faucon, M.; Saucerotte, B.; Zorz, N.; Moisy, P. *Dalton Trans.* **2006**, 2526–2534.
(30) Bosse, E.; Berthon, L.; Zorz, N.; Monget, J.; Berthon, C.; Bisel, I.; Legand, S.; Moisy, P. *Dalton Trans.* **2008**, 924–931.
(31) Le Rouzo, G.; Lamouroux, C.; Dauvois, V.; Dannoux, A.; Legand, S.; Durand, D.; Moisy, P.; Moutiers, G. *Dalton Trans.* **2009**, 6175–6184.
(32) Wishart, J. F.; Shkrob, I. A. In *Ionic Liquids: From Knowledge to Application*; Rogers, R. D., Plechkova, N. V., Seddon, K. R., Eds.; American Chemical Society: Washington, DC, 2009; pp 119−134.
(33) Shkrob, I. A.; Marin, T. W.; Chemerisov, S. D.; Hatcher, J.; Wishart, J. F. *J. Phys. Chem. B* **2011**10.1021/jp200305b.
(34) Markham, J. J. *F-centers in alkali halides*; Academic Press: New York, 1966.
(35) Wishart, J. F.; Neta, P. *J. Phys. Chem. B* **2003**, *107*, 7261–7267.
(36) Funston, A. M.; Wishart, J. F. In *Ionic Liquids IIIA: Fundamentals, Progress, Challenges, and Opportunities, Properties and Structure*, Rogers, R. D., Seddon, K. R., Eds.; American Chemical Society: Washington, DC, 2005; Vol. 901, pp 102−116.
(37) Wishart, J. F.; Lall-Ramnarine, S. I.; Raju, R.; Scumpia, A.; Bellevue, S.; Ragbir, R.; Engel, R. *Radiat. Phys. Chem.* **2005**, *72*, 99–104.
(38) Wishart, J. F. In *Ionic Liquids UnCOILed*; Rogers, R. D., Plechkova, N. V., Seddon, K. R., Eds.; Wiley, Ltd.: Chichester, U.K., 2011, in press.
(39) Chandrasekhar, N.; Schalk, O.; Unterreiner, A.-N. *J. Phys. Chem. B* **2008**, *112*, 15718–15724. Chandrasekhar, N.; Unterreiner, A.-N. *Phys. Chem. Chem. Phys.* **2010**, *12*, 1698.
(40) (a) For oxidative decarboxylation, see: Serguchev, Yu. A.; Beletskaya *Russ. Chem. Rev.* **1980**, *49*, 1119–11334. Tanner, D. D.; Osman, A. A. *J. Org. Chem.* **1987**, *52*, 4689–4693. (b) Chateauneuf, J.; Lusztyk, J.; Ingold, K. U. *J. Am. Chem. Soc.* **1987**, *109*, 897−899; **1988**, *110*, 2877−2885; **1988**, *110*, 2886−2893. Korth, H. G.; Chateauneuf, J.; Lusztyk, J.; Ingold, K. U. *J. Am. Chem. Soc.* **1988**, *110*, 5929–5931.
(41) Giernoth, R.; Bankmann, D. *Tetrahedron Lett.* **2006**, *47*, 4293–4296.
(42) Egorov, V. M.; Djigailo, D. I.; Momotenko, D. S.; Chernyshov, D. V.; Torocheshnikova, I. I.; Smirnova, S. V.; Pletnev, I. V. *Talanta* **2010**, *80*, 1177–1182.
(43) Shkrob, I. A.; Chemerisov, S. D. *J. Phys. Chem. C* **2009**, *113*, 17138.
(44) Becke, A. D. *Phys. Rev. A* **1988**, *38*, 3098. Lee, C.; Yang, W.; Parr, R. G. *Phys. Rev. B* **1988**, *37*, 785.
(45) Frisch, M. J.; Trucks, G. W.; Schlegel, H. B.; Scuseria, G. E.; Robb, M. A.; Cheeseman, J. R.; Zakrzewski, V. G.; Montgomery, J. A., Jr.; Stratmann, R. E.; Burant, J. C.; Dapprich, S.; Millam, J. M.; Daniels, A. D.; Kudin, K. N.; Strain, M. C.; Farkas, O.; Tomasi, J.; Barone, V.; Cossi, M.; Cammi, R.; Mennucci, B.; Pomelli, C.; Adamo, C.; Clifford, S.; Ochterski, J.; Petersson, G. A.; Ayala, P. Y.; Cui, Q.; Morokuma, K.; Malick, D. K.; Rabuck, A. D.; Raghavachari, K.; Foresman, J. B; Cioslowski, J.; Ortiz, J. V.; Baboul, A. G.; Stefanov, B. B.; Liu, G.; Liashenko, A.; Piskorz, P.; Komaromi, I.; Gomperts, R.; Martin, R. L.; Fox, D. J.; Keith, T.; Al-Laham, M. A.; Peng, C. Y.; Nanayakkara, A.; Gonzalez, C.; Challacombe, M.; Gill, P. M. W.; Johnson, B. G.; Chen, W.; Wong, M. W.; Andres, J. L.; Head- Gordon, M.; Replogle, E. S.; Pople, J. A. *Gaussian 98*, rev. A.1; Gaussian, Inc.: Pittsburgh, PA, 1998.
(46) Grodkowski, J.; Neta, P. *J. Phys. Chem. A* **2002**, *106*, 11130–11134. See also: Katoh, R.; Takahashi, K. *Radiat. Phys. Chem.* **2009**, *78*, 1126–1128.
(47) (a) Grodkowski, J.; Nyga, M.; Mirkowski, J. *Nukleonika* **2005**, *50*, S35–S38. (b) Marcinek, A.; Zielonka, J.; Gebicki, J.; Gordon, C. M.; Dunkin, I. R. *J. Phys. Chem. A* **2001**, *105*, 9305–9309.
(48) *Handbook of Chemistry and Physics*, 69th ed.; CRC Press: Boca Raton, FL, 1989; pp F−183.
(49) (a) Allen, D.; Baston, G.; Bradley, A. E.; Gorman, T.; Haile, A.; Hamblett, I.; Hatter, J. E.; Healey, M. J. F.; Hodgson, B.; Lewin, R.; Lovell, K. V.; Newton, B.; Pitner, W. R.; Rooney, D. W.; Sanders, D.; Seddon, K. R.; Sims, H. E.; Thied, R. C. *Green Chem.* **2002**, *4*, 152–158. (b) Padilla, J.; de Maria Ramirez, F. *J. Radioanal. Nucl. Chem.* **1999**, *242*, 653 and references therein. (c) Katsumura, Y.; Jiang, P. Y.; Naganishi, R.; Oishi, T.; Ishigure, K.; Yoshida, Y. *J. Phys. Chem.* **1991**, *95*, 4435–4439. Cook, A. R.; Dimitrijevic, N. D.; Dreyfus, B. W.; Meisel, D.; Curtiss, L. A.; Camaioni, D. M. *J. Phys. Chem. A* **2001**, *105*, 3658–3666.
(50) Rollins, A. W.; Kiendler-Scharr, A.; Fry, J. L.; Brauers, T.; Brown, S. S.; Dorn, H.-P.; Dube, W. P.; Fuchs, H.; Mensah, A.; Mentel, T. F.; Rohrer, F.; Tillmann, R.; Wegener, R.; Wooldridge, P. J.; Cohen, R. C. *Atmos. Chem. Phys.* **2009**, *9*, 6685–6703.

(51) (a) Nelson, D.; Symons, M. C. R. *J. Chem. Soc., Perkin Trans. 2* **1977**, 286–293. (b) Steenken, S.; Goldbergerova, L. *J. Am. Chem. Soc.* **1998**, *120*, 3298–3934. (c) Bernhard, W. A.; Ezra, F. S. *J. Phys. Chem.* **1974**, *78*, 958–961.
(52) von Ahsen, S.; Francisco, J. S. *Angew. Chem., Int. Ed.* **2004**, *43*, 3330–3333.
(53) Nelsen, S. F. *J. Am. Chem. Soc.* **1967**, *89*, 5256. Kasai, P. H. *J. Am. Chem. Soc.* **1992**, *114*, 2875–2880.
(54) Lind, J.; Jonsson, M.; Eriksen, T. E.; Merenyi, G.; Eberson, L. *J. Phys. Chem.* **1993**, *97*, 1610.
(55) Yashutskii, V. G.; Kovtun, V. Y. *Russ. Chem. Rev.* **1985**, *54*, 76–97.
(56) Chatdilialoglu, C.; Gilbert, B. C.; Kirk, C. M.; Norman, R. O. C. *J. Chem. Soc., Perkin Trans 2* **1978**, 1084.
(57) Kvaskoff, D.; Bednarek, P.; George, L.; Waich, K.; Wentrup *J. Org. Chem.* **2006**, *71*, 4049. Wijeratne, N. R.; Wenthold, P. G. *J. Am. Soc. Mass Spectrom.* **2007**, *18*, 2014.
(58) Rothe, E. W.; Mathur, B. P.; Reck, G. P. *Inorg. Chem.* **1980**, *19*, 829–831.
(59) Francisco, J. S.; Richardson, S. L. *J. Chem. Phys.* **1995**, *102*, 1100.